BOSE–EINSTEIN CORRELATIONS IN Z FRAGMENTATION AND OTHER REACTIONS*

Wolfram Kittel

HEFIN, University of Nijmegen/NIKHEF
Toernooiveld 1, 6525 ED Nijmegen, The Netherlands

(Received October 1, 2001)

Recent experimental studies of Bose–Einstein Correlations in Z fragmentation are reviewed in view of the need to understand their apparent suppression for pions originating from different W's. Particular features discussed are source elongation, position-momentum correlation, non-Gaussian shape of the correlator, transverse-mass dependence, density dependence and dilution, space–time shape of the emission function, neutral-pion and genuine higher-order correlations.

PACS numbers: 13.65.+i

1. Introduction

As proposed by Hanbury Brown and Twiss [1] in 1954, the (angular) diameter of stars and radio sources in the universe was successfully determined by measuring the intensity correlations between separated telescopes. Likewise, in particle physics, one can in principle use Bose–Einstein correlations between identical bosons to measure the space–time structure of the region from which particles originate in a high-energy collision [2], provided these bosons are produced incoherently.

The first experimental evidence for Bose–Einstein correlations in particle physics dates back to 1959 when, in $p\bar{p}$ annihilation at 1.05 GeV/c, Goldhaber *et al.* [3] observed an enhancement at small relative angles in like-sign pion pairs not present for unlike-sign pairs. More recently, Bose–Einstein correlations have been exploited in hadron–hadron, hadron–nucleus, nucleus–nucleus, e^+e^- and lepton–hadron collisions to obtain surprisingly detailed information on the space–time development of particle production.

* Presented at the XLI Cracow School of Theoretical Physics, Zakopane, Poland June 2–11, 2001.

The recent revival of interest comes from various directions:

1. Their application to determine the space–time development of a particle collision.

2. Their influence on the measurement of effective masses, in particular of the W mass at LEP2 [4,5].

3. Their role in the phenomenon of intermittency [6, 7].

4. Their possible effect on multiplicity distribution and single-particle spectra [8–10].

In this paper, we shall review recent experimental studies on the first point, in particular for e^+e^- collisions leading to hadronic final states at the Z energy. We consider this information crucial for an understanding of the underlying dynamics, and in particular of the apparent suppression of Bose–Einstein correlations of pions originating from different W's within the same event.

2. The correlation formalism

We start by defining symmetrized inclusive q-particle distributions

$$\rho_q(p_1,\ldots,p_q) = \frac{1}{\sigma_{\rm tot}} \frac{d\sigma_q(p_1,\ldots,p_q)}{\prod_1^q dp_q}\,, \tag{1}$$

where $\sigma_q(p_1,\ldots,p_q)$ is the inclusive cross section for q particles to be at $p_1,\ldots,p_q$, irrespective of the presence and location of any further particles, p_i is the (four-) momentum of particle i and $\sigma_{\rm tot}$ is the total hadronic cross section of the collision under study.

For the case of identical particles, integration over an interval Ω in p-space yields

$$\begin{aligned}
&\int_\Omega \rho_1(p)dp = \langle n\rangle\,,\\
&\int_\Omega\int_\Omega \rho_2(p_1,p_2)dp_1dp_2 = \langle n(n-1)\rangle\,,\\
&\int_\Omega dp_1 \ldots \int_\Omega dp_q \rho_q(p_1,\ldots,p_q) = \langle n(n-1)\ldots(n-q+1)\rangle\,,
\end{aligned} \tag{2}$$

where n is the multiplicity of identical particles within Ω in a given event and the angular brackets imply the average over the event ensemble.

Besides the interparticle *correlations* we are looking for, the inclusive q-particle number densities $\rho_q(p_1,\ldots,p_q)$ in general contain "trivial" contributions from lower-order densities. It is, therefore, advantageous to consider a new sequence of functions $C_q(p_1,\ldots,p_q)$ as those statistical quantities which vanish whenever one of their arguments becomes statistically independent of the others. Deviations of these functions from zero shall be addressed as *genuine* correlations.

The quantities with the desired properties are the correlation functions — also called (factorial) cumulant functions — or, in integrated form, Thiele's semi-invariants [11]. A formal proof of this property was given by Kubo [12]. The cumulant correlation functions are defined as in the cluster expansion familiar from statistical mechanics via the sequence [13–15]:

$$\rho_1(1) = C_1(1), \tag{3}$$

$$\rho_2(1,2) = C_1(1)C_1(2) + C_2(1,2), \tag{4}$$

$$\begin{aligned}\rho_3(1,2,3) &= C_1(1)C_1(2)C_1(3) + C_1(1)C_2(2,3) + C_1(2)C_2(1,3)\\ &\quad + C_1(3)C_2(1,2) + C_3(1,2,3);\end{aligned} \tag{5}$$

and, in general, by

$$\begin{aligned}\rho_m(1,\ldots,m) = \sum_{\{l_i\}_m} \sum_{\text{perm.}} &\underbrace{[C_1()\cdots C_1()]}_{l_1\,\text{factors}} \underbrace{[C_2(,)\cdots C_2(,)]}_{l_2\,\text{factors}}\\ &\cdots \underbrace{[C_m(,\ldots,)\cdots C_m(,\ldots,)]}_{l_m\,\text{factors}}.\end{aligned} \tag{6}$$

Here, l_i is either zero or a positive integer and the sets of integers $\{l_i\}_m$ satisfy the condition

$$\sum_{i=1}^{m} i\, l_i = m. \tag{7}$$

The arguments in the C_i functions are to be filled by the m possible momenta in any order. The sum over permutations is a sum over all distinct ways of filling these arguments. For any given factor product there are precisely [14]

$$\frac{m!}{[(1!)^{l_1}(2!)^{l_2}\cdots(m!)^{l_m}]\, l_1! l_2!\cdots l_m!} \tag{8}$$

terms.

The relations (6) may be inverted with the result:

$$\begin{aligned} C_2(1,2) &= \rho_2(1,2) - \rho_1(1)\rho_1(2)\,, \\ C_3(1,2,3) &= \rho_3(1,2,3) - \sum_{(3)} \rho_1(1)\rho_2(2,3) + 2\rho_1(1)\rho_1(2)\rho_1(3)\,, \\ C_4(1,2,3,4) &= \rho_4(1,2,3,4) - \sum_{(4)} \rho_1(1)\rho_3(1,2,3) - \sum_{(3)} \rho_2(1,2)\rho_2(3,4) \\ &\quad + 2\sum_{(6)} \rho_1(1)\rho_1(2)\rho_2(3,4) - 6\rho_1(1)\rho_1(2)\rho_1(3)\rho_1(4)\,, \end{aligned} \tag{9}$$

etc. In the above relations we have abbreviated $C_q(p_1,\ldots,p_q)$ to $C_q(1,2,\ldots,q)$; the summations indicate that all possible permutations must be taken (the number under the summation sign indicates the number of terms). Expressions for higher orders can be derived from the related formulae given in [16].

It is often convenient to divide the functions ρ_q and C_q by the product of one-particle densities, which leads to the definition of the normalized inclusive densities and correlations:

$$R_q(p_1,\ldots,p_q) = \rho_q(p_q,\ldots,p_q)/\rho_1(p_1)\ldots\rho_1(p_q)\,, \tag{10}$$

$$K_q(p_1,\ldots,p_q) = C_q(p_1,\ldots,p_q)/\rho_1(p_1)\ldots\rho_1(p_q)\,. \tag{11}$$

In terms of these functions, correlations have been studied extensively for $q=2$. Results also exist for $q=3$, but usually the statistics (*i.e.*, number of events available for analysis) are too small to isolate genuine correlations. To be able to do that for $q \geq 3$, one must apply moments defined via the integrals in Eq. (2), but in limited phase-space cells [6].

3. Alternative views

3.1. Pion interferometry

In Fig. 1 we illustrate the production of two identical pions with momenta $\boldsymbol{p}_1$ and $\boldsymbol{p}_2$, arising from two sources A and B with coordinates $\boldsymbol{x}_\mathrm{A}$, $\boldsymbol{x}_\mathrm{B}$ (see also [17]). The pion wave functions can be written as

$$\psi_{1\mathrm{A}} = \mathrm{e}^{-i\boldsymbol{p}_1\cdot\boldsymbol{x}_\mathrm{A}+i\alpha}\,, \qquad \psi_{2\mathrm{B}} = \mathrm{e}^{-i\boldsymbol{p}_2\cdot\boldsymbol{x}_\mathrm{B}+i\beta} \tag{12}$$

if $\pi(\boldsymbol{p}_1)$ is emitted from source A and $\pi(\boldsymbol{p}_2)$ from source B, where α and β are arbitrary phases of the sources.

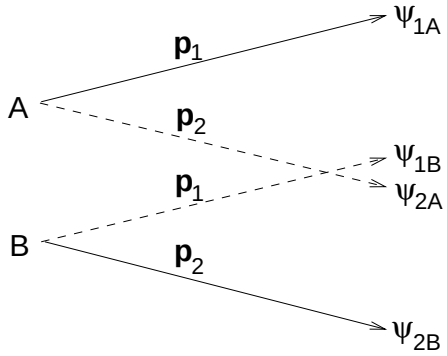


Fig. 1. Emission of two identical bosons with momenta $\boldsymbol{p}_1, \boldsymbol{p}_2$ from two sources A, B.

If $\pi(\boldsymbol{p}_1)$ is emitted from source B and $\pi(\boldsymbol{p}_2)$ from source A, then indices A and B (and the phases) should be interchanged in (12). Since the two pions are identical bosons and the observer cannot decide from which source a particular pion was emitted, the coincidence amplitude for simultaneous observation of two pions with momenta $\boldsymbol{p}_1$ and $\boldsymbol{p}_2$ has to be Bose-symmetrized:

$$A_{\mathrm{BE}} = \psi_{1\mathrm{A}}\psi_{2\mathrm{B}} + \psi_{1\mathrm{B}}\psi_{2\mathrm{A}} \ . \tag{13}$$

The corresponding coincidence rate is

$$I_{\mathrm{BE}} = |A_{\mathrm{BE}}|^2 = 2 + 2\cos(\Delta\boldsymbol{p} \cdot \Delta\boldsymbol{x}) \, , \tag{14}$$

where $\Delta\boldsymbol{p} = \boldsymbol{p}_1 - \boldsymbol{p}_2$ and $\Delta\boldsymbol{x} = \boldsymbol{x}_{\mathrm{A}} - \boldsymbol{x}_{\mathrm{B}}$. Note that the arbitrary phases α, β have dropped out from (14), which is valid for completely incoherent emission. We define as two-particle Bose–Einstein ratio R_2 the ratio between I_{BE} and the rate I_0 which would be observed if there were no BE interference:

$$R_2 = \frac{I_{\mathrm{BE}}}{I_0} = 1 + \cos(\Delta\boldsymbol{p} \cdot \Delta\boldsymbol{x}) \, . \tag{15}$$

From (15) it follows that R_2 reaches a maximum value of 2 for $\Delta\boldsymbol{p} = 0$. Furthermore, it can be seen that the momentum difference $\Delta\boldsymbol{p}$ probes the source dimensions in a direction parallel to $\Delta\boldsymbol{p}$.

We shall, however, see later on that such a simple picture cannot be maintained due to correlation between $\boldsymbol{x}$ and $\boldsymbol{p}$ observed in the data and expected from hydrodynamical models as well as from string models.

One step more realistic than the binary source considered in Fig. 1 is a source with a spherically symmetric Gaussian density distribution of emitting centers [3]

$$\rho(\boldsymbol{r}) \propto \exp\left[\frac{-\boldsymbol{r}^2}{2r_0^2}\right] \, , \tag{16}$$

which yields as Bose–Einstein ratio

$$R_2 = 1 + \exp\left[-r_0^2 \Delta \boldsymbol{p}^2\right] . \tag{17}$$

or, in its Lorentz-invariant form,

$$R_2(Q^2) = 1 + \exp(-r_{\mathrm{G}}^2 Q^2)$$

with

$$Q^2 \ = -(p_1 - p_2)^2 = M^2 - 4m_\pi^2 , \tag{18}$$

where M is the invariant mass of the pion pair. This corresponds to a Gaussian shape of the source in the center-of-mass system of the pair, where $q_0 \equiv \Delta E = 0$.

3.2. Emission function and Wigner function

The picture presented in Sect. 3.1 corresponds to the one-dimensional treatment of a spherically symmetric static source. However, a high-energy collision is neither spherically symmetric nor static. A formalism particularly handy for the fully-dimensional treatment of a dynamical emitter is the so-called Wigner-function formalism [18–19]. This is based on the emission function $S(x,p)$, a covariant Wigner-transform of the source density matrix. $S(x,p)$ can be interpreted as a quantum-mechanical analogue of the classical probability that a boson is produced at a given space–time point $x = (t, \boldsymbol{r})$ with a given momentum-energy $p = (E, \boldsymbol{p})$.

In the general case, the normalized two-particle density $R_2(1,2)$ or correlation function $K_2(1,2)$ depend on the momentum components of particles 1 and 2. For the study of correlations, it is convenient to decompose the two single-particle four-vectors p_1 and p_2 into the average $K = [(E_1 + E_2)/2,\ \boldsymbol{K} = \boldsymbol{p}_1 + \boldsymbol{p}_2)/2]$ and the relative momentum $Q = (\Delta E = E_1 - E_2, \boldsymbol{Q} = \boldsymbol{p}_1 - \boldsymbol{p}_2)$.

Starting from the space–time x and momentum-energy K dependent pion-emission function $S(x,K)$, the normalized density in momentum space can be written as [19]

$$R_2(\boldsymbol{Q}, \boldsymbol{K}) \approx 1 + \frac{|\int d^4x S(x,K) \mathrm{e}^{iQ\cdot x}|^2}{|\int d^4x S(x,K)|^2} = 1 + |\langle \mathrm{e}^{iQ\cdot x}\rangle|^2 . \tag{19}$$

In a Gaussian approximation around the mean space–time production point $\bar{x}$,

$$R_2(\boldsymbol{Q}, \boldsymbol{K}) = 1 + \exp[-Q_\mu Q_\nu \langle (x-\bar{x})_\mu (x-\bar{x})_\nu \rangle (\boldsymbol{K})] + \delta R_2(\boldsymbol{Q}, \boldsymbol{K}) . \tag{20}$$

The variances $\langle (x-\bar{x})_\mu (x-\bar{x})_\nu \rangle$ give the size of the space–time region from which pions of similar momentum are emitted (which, for Gaussian sources, coincides with the more general concept [20] of *lengths of homogeneity*) and δR_2 contains all non-Gaussian contributions, usually assumed to be small.

Since the four-momenta p_i of the two particles are on-shell, Q and K are in general off-shell but obey the orthogonality and mass-shell constraints

$$Q \cdot K = 0\,, \qquad K^2 - \frac{Q^2}{4} = m^2\,, \tag{21}$$

so that only 6 linear combinations of the variances are measurable [21]. If the source is azimuthally symmetric in coordinate space, a reflection symmetry is present in momentum space with respect to the plane spanned by $\boldsymbol{K}$ and the event axis. As a consequence, all mixed variances linear in the direction orthogonal to this plane ("sidewards") must vanish and the correlator must be symmetric under $Q_{\rm side} \to -Q_{\rm side}$, so that only four linear combinations remain measurable! Note, however, that every one of them depends on $\boldsymbol{K}$.

3.3. String models

Alternatively, Bose–Einstein correlations have been introduced into string models [22–24]. In these models, an ordering in space–time exists for the hadron momenta within a string. Bosons close in phase space are nearby in space–time and the length scale measured by Bose–Einstein correlations is not the full length of the string, but the distance in boson-production points for which the momentum distributions still overlap.

Fig. 2(a) illustrates the production of (identical) particles 1 and 2 from a color string in x and t. The color field breaks up into quark-antiquark pairs and adjacent quarks and antiquarks recombine into mesons. The production of the same final state, but with particles 1 and 2 exchanged is described in Fig. 2(b).

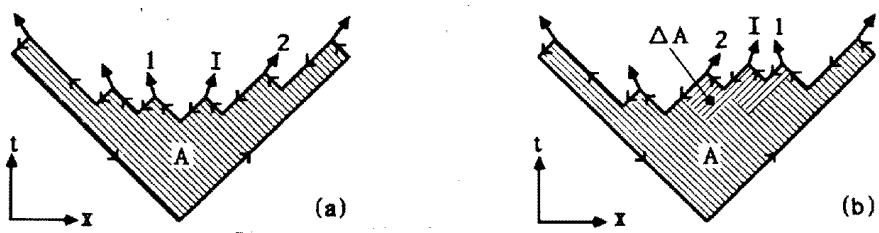


Fig. 2. Space-time diagram for two ways to produce two identical bosons in the color-string picture [23].

In a color-string model, the (non-normalized) probability $d\Gamma_n$ to produce an n-particle state $\{p_j\}$, $j = 1, \ldots n$ of distinguishable particles is

$$d\Gamma_n = [\Pi_{j=1}^{n} N dp_j \delta(p_j^2 - m_j^2)] \delta(\Sigma p_j - P) \exp(-bA_n) \ , \tag{22}$$

where the exponential factor can be interpreted as the square of a matrix element

$$M_n = \exp(i\xi A_n) \, , \quad \mathrm{Re}(\xi) = \kappa \, , \quad \mathrm{Im}(\xi) = \frac{b}{2} \, , \tag{23}$$

and the remaining terms describe longitudinal phase space, with P being the total energy-momentum of the state. N is related to the mean multiplicity and b to the correlation length in rapidity. A_n corresponds to the total space–time area covered by the color field (Fig. 2), or to an equivalent area in energy-momentum space divided by the square of the string tension $\kappa = 1$ GeV/fm [23].

The production of two identical bosons (1,2) is governed by the symmetric matrix element

$$M = \frac{1}{\sqrt{2}}(M_{12} + M_{21}) = \frac{1}{\sqrt{2}}[\exp(i\xi A_{12}) + \exp(i\xi A_{21})] \ . \tag{24}$$

From Fig. 2 it is clear that there is an area difference and, consequently, a phase difference between M_{12} and M_{21} of

$$\Delta A = |A_{12} - A_{21}| = \frac{1}{\kappa^2} |\boldsymbol{p}_1 E_2 - \boldsymbol{p}_2 E_1 + (\boldsymbol{p}_1 - \boldsymbol{p}_2) E_{\mathrm{I}} - (E_1 - E_2) \boldsymbol{p}_{\mathrm{I}}| \, , \tag{25}$$

where the indices 1,2 and I represent particles 1, 2 and system I, respectively.

Using this matrix element, one obtains

$$R_{\mathrm{BE}} \approx 1 + \left\langle \frac{\cos(\kappa \Delta A)}{\cosh \frac{b \Delta A}{2}} \right\rangle \quad , \tag{26}$$

where the average runs over all I. In the limit $Q^2 = -(p_1 - p_2)^2 = 0$, (25) gives $\Delta A = 0$ and (26) $R_{\mathrm{BE}} = 2$, in agreement with the results from the conventional interpretation for completely incoherent sources. However, for $Q^2 \neq 0$ follows an additional dependence on the momentum p_{I} of the system I produced between the two bosons.

Corrections to (26) are necessary due to non-zero mass and transverse momentum of quarks and due to the contribution of resonances to the production of particles of type 1, 2.

The model can account well for most features of the e^+e^- data [25–27], including the approximately spherical shape of the BE effect. More recently, the symmetrization has been generalized to more than 2 identical particles [28].

4. Recent experimental results

4.1. Existence

Bose–Einstein correlations are by now a well established effect in the hadronic final states of Z decay [29–31]. A clear enhancement is observed in R_2 at small Q. This is not a trivial observation since, according to the pion interferometry interpretation of Sect. 3.1, this would require at least partially chaotic pion production.

If present in hadronic Z final states, there is no reason to expect it to be absent in hadronic W final states (intra-W BEC), and a signal consistent with that of Z into light quarks is indeed established [32]. Examples for R_2 as a function of Q are given in Fig. 3, both for W and Z fragmentation.

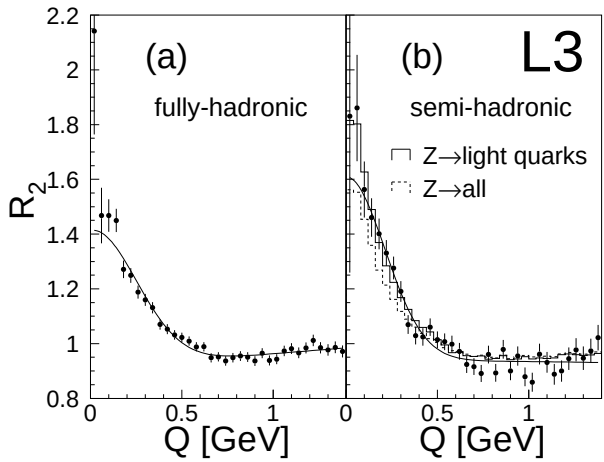


Fig. 3. The Bose–Einstein correlation function R_2 for (a) the fully-hadronic WW events, and (b) the semi-hadronic WW events. In (b) the full histogram is for the light-quark Z decay sample and the dashed histogram is for a sample containing all hadronic Z decays. Also shown are Gaussian fits to the WW data [32].

The important question is that of BEC between pions each originating from a different W in fully hadronic W^+W^- final states (inter-W BEC). If existent, such a correlation would, on the one hand, cause a potential bias in the mass determination of the W [4,5]. On the other, it could serve as a pion-interferometry laboratory for the measurement of the space–time development of W fragmentation into pions. The recent status of the search for inter-W BEC is covered in [33].

For a detailed understanding of W^+W^- overlap and inter-W BEC, a detailed analysis of BEC in a single W would be required. Given that only a few thousand of these W's have been produced at LEP, such a detailed study is presently not possible. It is, however, possible on the millions of

events accumulated at the Z, and we shall assume that the fragmentation properties are similar for those two bosons (except for the fact that $Z \to b\bar{b}$ has no equivalent in W decay). Since this detailed analysis is still going on, we shall also look at corresponding properties in hadron–hadron and even heavy-ion collisions.

4.2. Pion-source elongation

The form of the correlation function in more than one dimension has been a major subject of theoretical study in recent years [19,28,34–38]. In Monte Carlo generators, spherical symmetry is usually assumed [5, 39–41], while elongation can be expected when a string-like shape is maintained [28,38]. Experimentally, detailed three-dimensional analyzes were done for heavy-ion collisions [42,43] and for hadron–hadron collisions [44]. While the volume of the pion emission region appeared to be approximately spherical for heavy-ion collisions, a clear elongation was observed in hadron–hadron collisions. An elongation is now also observed at LEP [45–47].

In this analysis the longitudinal center-of-mass system (LCMS) [36] is used. This is defined for each pair of particles as the system, resulting from a boost along the thrust axis, in which the sum of the momenta of the pair is perpendicular to the thrust axis. In this system, one can resolve the three-momentum difference of the pair of particles into a longitudinal component Q_{L} parallel to the thrust axis, Q_{out} along the sum of the particles' momenta (see Fig. 4) and Q_{side} perpendicular to both Q_{L} and Q_{out}. Then, the invariant four-momentum difference can be written as [36]

$$Q^2 = Q_{\mathrm{L}}^2 + Q_{\mathrm{side}}^2 + Q_{\mathrm{out}}^2 - (\Delta E)^2 = Q_{\mathrm{L}}^2 + Q_{\mathrm{side}}^2 + Q_{\mathrm{out}}^2(1-\beta^2), \tag{27}$$

where

$$\beta \equiv \frac{p_{\mathrm{out}\,1} + p_{\mathrm{out}\,2}}{E_1 + E_2} \tag{28}$$

with $p_{\mathrm{out}\,i}$ and E_i $(i = 1, 2)$ the out-component of the momentum and the energy, respectively, of particle i in the LCMS. The energy difference ΔE and, therefore, the difference in emission time of the two particles couples only to the component Q_{out}. Consequently, Q_{L} and Q_{side} reflect only spatial dimensions of the source, whereas Q_{out} reflects a mixture of spatial and temporal dimensions. The correlation function is then parametrized in terms of $\boldsymbol{Q} = (Q_{\mathrm{L}}, Q_{\mathrm{side}}, Q_{\mathrm{out}})$:

$$R_2(\boldsymbol{Q}) = \frac{\rho_2(\boldsymbol{Q})}{\rho_0(\boldsymbol{Q})}. \tag{29}$$

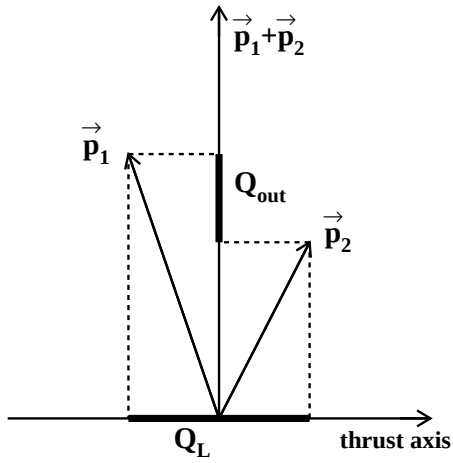


Fig. 4. The longitudinal center of mass frame (LCMS) showing the projection of Q on the ($Q_{\rm L}$–$Q_{\rm out}$) plane. $Q_{\rm side}$ is the projection of Q on the axis perpendicular to this plane.

Assuming a Gaussian (azimuthally, but not necessarily spherically, symmetric) shape of the source, the following three-dimensional parametrization has been proposed [19,35,48]:

$$R_2(Q_{\rm L},Q_{\rm out},Q_{\rm side}) = \gamma\,(1+\delta Q_{\rm L}+\varepsilon Q_{\rm out}+\xi Q_{\rm side}) \times\left[1+\lambda\exp\left(-R_{\rm L}^2Q_{\rm L}^2-R_{\rm out}^2Q_{\rm out}^2-R_{\rm side}^2Q_{\rm side}^2+2\rho_{\rm L,out}R_{\rm L}R_{\rm out}Q_{\rm L}Q_{\rm out}\right)\right], \tag{30}$$

where the factor $(1+\delta Q_{\rm L}+\varepsilon Q_{\rm out}+\xi Q_{\rm side})$ takes into account possible long-range momentum correlations in the form of a slow rise, γ is a normalization factor close to unity and the term between square brackets is the two-particle Bose–Einstein correlation function associated with a Gaussian shape of the source.

By fitting the correlation function with this parametrization, one can extract the factor λ, which measures the strength of the correlation, and the 'radii' r_i ($i=$ L, out and side) defined as $\sigma_i/\sqrt{2}$, with the σ_i^2 the variances of a multi-dimensional Gaussian distribution of the source in configuration space. $\rho_{\rm L,out}$ is the correlation between the longitudinal and out components of this Gaussian. In the LCMS, the duration of particle emission only couples to the out-direction and only enters in the parameters $R_{\rm out}$ and $\rho_{\rm L,out}$. Hence, $R_{\rm side}$ can be interpreted as the transverse component of the geometric radius. The parametrization, Eq. (30), assumes azimuthal symmetry of the source, which means that the two-particle Bose–Einstein correlation function associated with the Gaussian shape of the source, is invariant under the transformation

$Q_{\rm side} \to -Q_{\rm side}$. Consequently, the only possible off-diagonal term is the $Q_{\rm L}Q_{\rm out}$ term. It turns out to be zero within errors, however.

The results of three LEP experiments [45–47] are summarized in Table I. In spite of the different selection criteria and reference samples, all experiments consistently demonstrate an elongated shape of the pion source (or rather region of homogeneity) in hadronic Z decay. On the other hand, $r_{\rm side}/r_{\rm L} = 1.08 \pm 0.03$ is found [45] for JETSET with BE [49].

TABLE I

Elongation of the pion source in hadronic Z^0 decays: summary of the measurements at LEP1 ($r_{\rm T}$ corresponds to $Q_{\rm T} = \sqrt{Q_{\rm out}^2 + Q_{\rm side}^2}$).

	L3 "mixed" reference, all events	DELPHI "mixed" reference, 2-jet events	OPAL "+−" reference, 2-jet events
λ	$0.41 \pm 0.01^{+0.020}_{-0.019}$	$0.261 \pm 0.007 \pm 0.010$	0.443 ± 0.005
$r_{\rm L}$, fm	$0.74 \pm 0.02^{+0.04}_{-0.03}$	$0.85 \pm 0.02 \pm 0.07$	$0.989 \pm 0.011^{+0.030}_{-0.015}$
$r_{\rm out}$, fm	$0.53 \pm 0.02^{+0.05}_{-0.06}$		$0.647 \pm 0.011^{+0.024}_{-0.124}$
$r_{\rm side}$, fm	$0.59 \pm 0.01^{+0.03}_{-0.13}$		$0.809 \pm 0.009^{+0.019}_{-0.032}$
$r_{\rm side}/r_{\rm L}$	$0.80 \pm 0.02^{+0.03}_{-0.18}$		$0.818 \pm 0.018^{+0.008}_{-0.050}$
$r_{\rm T}$, fm		$0.53 \pm 0.02 \pm 0.07$	
$r_{\rm T}/r_{\rm L}$		$0.62 \pm 0.02 \pm 0.05$	

A systematic study of the hierarchy of radii obtained from JETSET was recently performed in [50]. Starting from a spherically symmetric Gaussian correlator, the authors obtain

$$r_{\rm side} > r_{\rm L} > r_{\rm out} \,,$$

unlike the experimentally observed elongation, both when using momentum shifting [49] or event weighting [51] to simulate the correlation. Generalizing to asymmetric weights, the experimentally observed elongation can be reproduced, but finding a good set of input radius parameters turns out an involved procedure.

What is important to realize is that the measured longitudinal radius has nothing to do with the elongation of the $q\bar{q}$ string stretched in Z decay. We shall see in Sect. 4.6 that the full pion-emission function is of the order

of 100 fm long, so that $r_{\rm L}$ only measures a small fraction of it. The reason for that is a strong $\boldsymbol{x}, \boldsymbol{p}$ correlation. Pions produced at a large distance on the string also have very different momenta and do not correlate. The "radii" therefore measure the effective size of the source segment radiating mesons with sufficiently small relative momentum (length of homogeneity), as shown in Fig. 5.

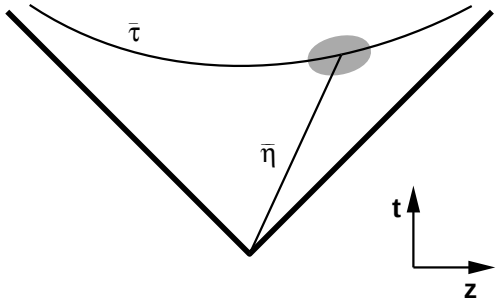


Fig. 5. Space-time picture of particle emission for a given fixed mean momentum of the pair. The mean value of the proper-time and the space–time rapidity distributions is denoted by $\overline{\tau}$ and $\overline{\eta}$. As the rapidity of the produced particles changes from the smallest to the largest possible value, the $[\overline{\tau}(y), \overline{\eta}(y)]$ variables scan the surface of mean particle production in the (t, z) plane [38].

4.3. The functional form of the correlation function

More important than the parameters extracted from "forcing" the two-particle correlation function into a fit by a pre-selected parametrization, is the actual experimentally observed shape of this distribution, itself.

The simple geometrical interpretation of the interference pattern based on the optical analogy as in Sect. 3.1 is invalid when emitters move relativistically with respect to each other, leading to strong correlations between the space–time and momentum-energy coordinates of emitted particles [52, 53]. Correlations of this type arise due to the nature of inside-outside cascade dynamics [54] as in color-string fragmentation [55]. In the interpretation of BEC by Andersson and Hofmann [23] in the string model, the length scale measured by BEC is therefore not related to the size of the total pion emitting source, but to the space–time separation between production points for which the momentum distributions still overlap. This distance is, in turn, related to the string tension. The model predicts an approximately exponential shape of the correlation function

$$R_2(Q) = R_0(1 + \lambda \exp(-rQ)) \ , \tag{31}$$

where r is expected to be independent of the total interaction energy.

Furthermore, scale-invariant dynamics is strongly connected with Bose–Einstein correlation. Scale invariance implies that multiparticle correlation functions exhibit power-law behavior over a considerable range of the relevant relative distance measure (such as Q^2) in phase space [6,7]. As such, BEC from a static source do not exhibit power-law behavior. However, a power law is obtained if the size of the particle source fluctuates event-by-event, and/or, if the source itself is a self-similar (fractal-like) object extending over a large volume [56]. In these studies, the ratio R_2 is parametrized using the form

$$R_2(M) = A + B\left(\frac{1}{Q^2}\right)^{\beta} . \tag{32}$$

The usually "reasonable" χ^2 values of the Gaussian fits hide the fact that the Gaussian parametrization in general fails at low values of Q^2, where statistical errors are often large. For the case of two-particle correlations, this has been demonstrated convincingly by NA22 [57] and UA1 [58], but deviations from a Gaussian are also observed in lepton–hadron [59,60] and e^+e^- [30] collisions.

This failure of a (multi-) Gaussian form persists in higher-order correlations. In Fig. 6(a) the NA22 data [61] on BE correlations of order $q = 2$ to 4 are plotted as a function of Q^2, in conventional linear scale. The curves are the fits by a q-fold Gaussian parametrization [62]. In Fig. 6(b) the same data and the same fits are repeated for $Q^2 < 1$ GeV^2 on ln–ln scale (where the Q^2 axis is reflected, *i.e.*, small Q^2 correspond to large $-\ln Q^2$). Even though the statistical errors at small Q^2 are large (the very reason why small Q^2 does not contribute much to χ^2), it is obvious that small-Q^2 points *systematically* lie higher than the multi-Gaussian fit, thus supporting a power-law behavior. This effect is even enhanced when the data are corrected for Coulomb repulsion.

Fig. 7(a) shows [63] the second-order cumulant K_2 as a function of Q (on log-scale) compared to a general quantum statistical model, based on a classical source current formalism applied successfully in quantum optics [64]. It includes as special cases more specific models such as [18] and [62]. The APW normalized cumulant predictions are built from normalized correlators d_{ij}, the on-shell Fourier transforms of classical space–time current correlators. The specific parametrizations tested in Fig. 7 are

$$\begin{aligned} \text{Gaussian}: &\quad d_{ij} = \exp(-r^2 Q_{ij}^2)\,, \\ \text{exponential}: &\quad d_{ij} = \exp(-r Q_{ij})\,, \\ \text{power law}: &\quad d_{ij} = Q_{ij}^{-\alpha}\,. \end{aligned} \tag{33}$$

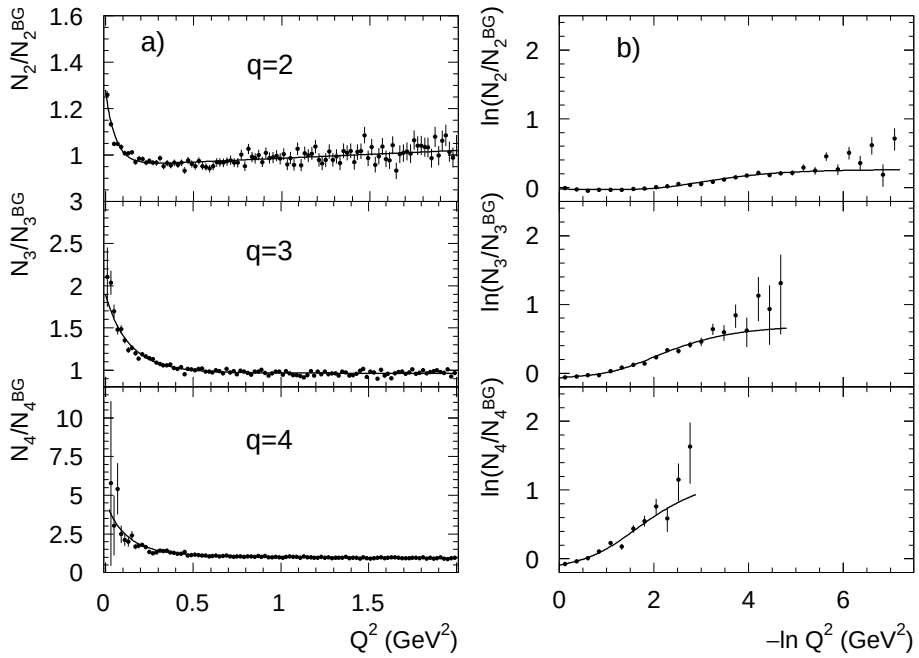


Fig. 6. The normalized two-, three- and four-particle inclusive densities as a function of Q^2 (left) and -lnQ^2 (right) [61]. Curves show the multi-Gaussian fits according to [62].

For constant chaoticity λ and real-valued currents, APW predict as second- and third-order normalized cumulants

$$K_2(Q_{12}) = 2\lambda(1-\lambda)d_{12} + \lambda^2 d_{12}^2\,, \tag{34}$$

$$K_3(Q_{12},Q_{23},Q_{31}) = 2\lambda^2(1-\lambda)[d_{12}d_{23}+d_{23}d_{31}+d_{31}d_{12}] + 2\lambda^3 d_{12}d_{23}d_{31}\,. \tag{35}$$

The fits in Fig. 7(a) contain an additive "background" parameter, in addition to λ and r as free parameters. The Gaussian fit is clearly excluded and the best fit is achieved with the power-law parametrization of the correlation function (full line).

Also K_3 plotted in Fig. 7(b) shows a power-law increase. It is, furthermore, visible in Fig. 7(b) that the increase is faster than expected from APW K_2, even for the power-law parametrization.

So, there is ample room for improvement of the models and we believe that the recently developed methods of studying the correlations (higher-order cumulants, higher dimensionality, alternative parametrizations of the correlation function) have opened the way for an improvement of these models.

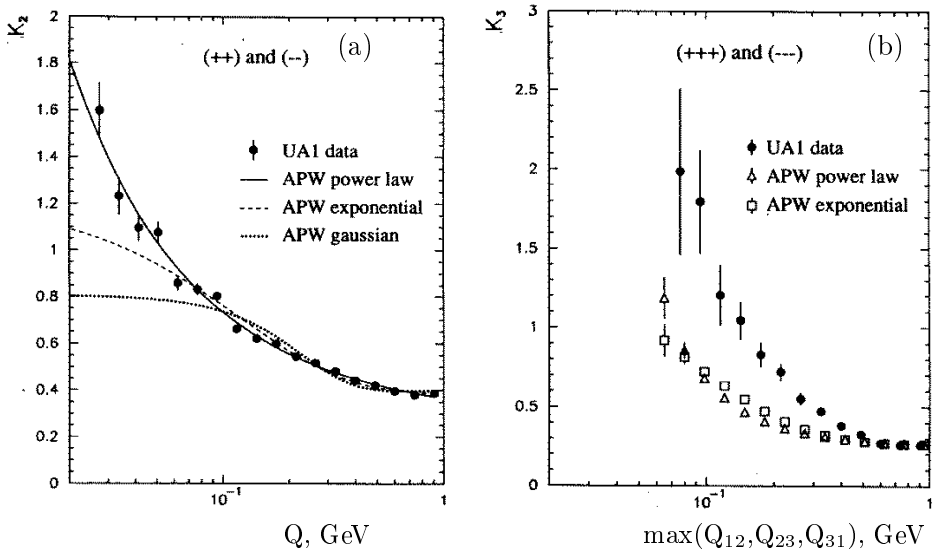


Fig. 7. (a) Second-order cumulant with fits of the forms given. (b) Third-order cumulant with APW predictions based on K_2 [63].

An interesting extension of the usual Gaussian approximation of the BE correlation function is an Edgeworth expansion [16] as suggested in [65]

$$R_2(Q) = \gamma \left(1 + \lambda^* \exp(-t^2/2) \left[1 + \frac{\kappa_3}{3!} H_3(t) + \frac{\kappa_4}{4!} H_4(t) + \ldots\right]\right) , \quad (36)$$

with $t = \sqrt{2} Q \cdot r$, H_n being the n-th Hermite polynomial, and κ_n the n-th order cumulant moment of the correlation function, where κ_2 yields r. The Hermite polynomials of odd order vanish at the origin, so that

$$\lambda = \lambda^* [1 + \kappa_4/8 + \ldots] . \quad (37)$$

A generalization to higher dimensions is straightforward [65], except for possible correlations between the Q_i variables.

The influence of the non-Gaussian shapes was studied [65] on AFS [66, 67], E802 [68] and NA44 [69] data. In Fig. 8, a Q_T projection of a 2D Edgeworth fit is compared to that of a 2D Gaussian fit to the E802 data. The deviation from a Gaussian (dashed) is obvious, and the Edgeworth expansion (full line) is flexible enough to describe it (with $\lambda = 1$!).

In Fig. 7(a) it was shown that even an exponential is not steep enough to reproduce the fast increase of K_2. An interesting observation of [65] is, that a Laguerre expansion of an exponential can reproduce these UA1 and the NA22 data (Fig. 9). However, at low Q^2 data are still systematically above the fit and a power-law fit is reported in [65] to give similarly

good χ^2/NDF with a smaller number of fit parameters. With a core-halo model [87] strength parameter of $\lambda_* = 1.14 \pm 0.10$ (UA1) and $\lambda_* = 1.11 \pm 0.17$ (NA22), *i.e.*, at maximum possible value (unity), there are either other than BE correlations at work or all resonances are resolved at these low Q^2 values. This may imply the connection between the observed power-law behavior (intermittency) and resonance contributions of BE correlations [56].

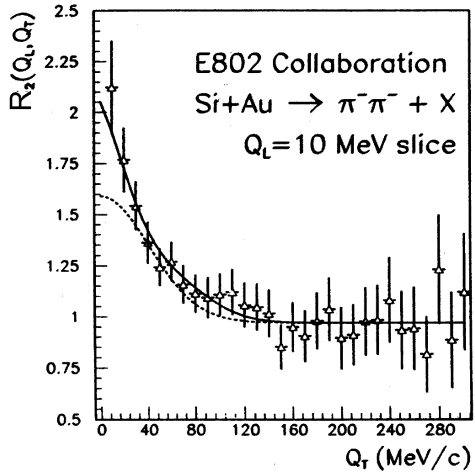


Fig. 8. Projection onto Q_{T} of a two-dimensional Gaussian (dashed) and Edgeworth (solid) fits for a small-Q_{L} slice [65].

In a 3D analysis of e^+e^- collisions at the Z-mass [45], results more satisfactory than those obtained with either Gaussian or exponential parametrizations were obtained with the Edgeworth expansion. Taking only the lowest-order non-Gaussian term into account (and dropping the off-diagonal term), Eq. (30) results in

$$
\begin{aligned}
&R_2(Q_{\mathrm{L}}, Q_{\mathrm{out}}, Q_{\mathrm{side}}) \\
&= \gamma\,(1 + \delta Q_{\mathrm{L}} + \varepsilon Q_{\mathrm{out}} + \xi Q_{\mathrm{side}}) \\
&\times \Big\{1 + \lambda \exp\left(-r_{\mathrm{L}}^2 Q_{\mathrm{L}}^2 - r_{\mathrm{out}}^2 Q_{\mathrm{out}}^2 - r_{\mathrm{side}}^2 Q_{\mathrm{side}}^2\right) \\
&\times \left[1 + \frac{\kappa_{\mathrm{L}}}{3!} H_3(R_{\mathrm{L}} Q_{\mathrm{L}})\right]\left[1 + \frac{\kappa_{\mathrm{out}}}{3!} H_3(R_{\mathrm{out}} Q_{\mathrm{out}})\right]\left[1 + \frac{\kappa_{\mathrm{side}}}{3!} H_3(R_{\mathrm{side}} Q_{\mathrm{side}})\right]\Big\}\,,
\end{aligned}
\tag{38}
$$

where κ_i ($i = \mathrm{L}, \mathrm{out}, \mathrm{side}$) is the third-order cumulant moment in the corresponding direction and $H_3(R_i Q_i) \equiv (\sqrt{2} R_i Q_i)^3 - 3\sqrt{2} R_i Q_i$ is the third-order Hermite polynomial. Note that the second-order cumulant corresponds to

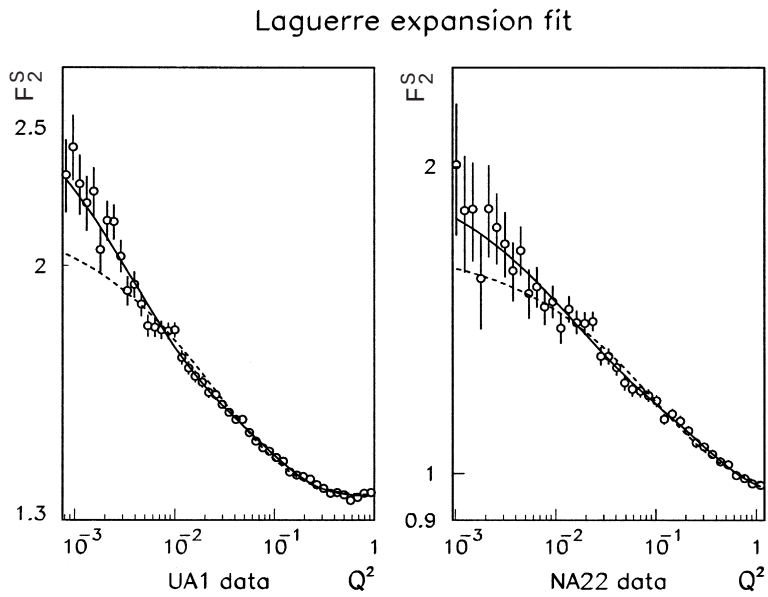


Fig. 9. The figures show F_2^s which is proportional to the two-particle Bose–Einstein correlation function, as measured by the UA1 [58] and the NA22 [57] Collaborations. The dashed lines stand for the exponential fit, the solid lines for that with the Laguerre expansion [65].

the radius r_i. Applying this expansion to the L3 data [45] discussed in Sect. 4.2 improves the confidence level of the fit from 3% to 30%. Non-zero values of the κ parameters indicate the deviation from a Gaussian, λ is larger than the corresponding Gaussian λ and the values of the radii confirm the elongation observed from the Gaussian fit.

4.4. (Transverse) mass dependence

4.4.1. The $K^{\pm}K^{\pm}$ system

Kaons are less affected by resonance decay than pions and could eventually provide a cleaner signal of the source. Bose–Einstein correlations among equally-charged kaons were observed in hh [71,72], AA [73,74] and e^+e^- [75,76] collisions (see Table II for the latter).

The size of the kaon emission region tends to be smaller than that of the pion emission region, in particular in AA collisions. The difference in resonance effects on $\pi\pi$ and KK correlations only partially can explain this difference in AA collisions. In e^+e^- collisions, the Gaussian radius parameter r_{G} tends to be smaller for $K^{\pm}K^{\pm}$ than for $\pi^{\pm}\pi^{\pm}$, but the spread is large due to different choices of background.

TABLE II

Parameters λ_G and r_G in the Gaussian parametrization in e^+e^- interactions at LEP, for different like-charged particles [76].

Pair	λ_G	r_G fm	Ref.	Selection	Ref. sample
$\pi^\pm\pi^\pm$	0.35 ± 0.04	0.42 ± 0.04	DELPHI [30]	2-jet	mixed
	0.40 ± 0.02	0.49 ± 0.02	ALEPH [31]	2-jet	mixed
	0.58 ± 0.01	0.79 ± 0.02	OPAL [77]	all	MC
$\pi^\pm\pi^\pm$	0.45 ± 0.02	0.82 ± 0.03	DELPHI [30]	all	unlike
	0.62 ± 0.04	0.81 ± 0.04	ALEPH [31]	2-jet	unlike
	$0.67 \pm 0.01 \pm 0.02$	$0.96 \pm 0.01 \pm 0.02$	OPAL [77]	all	unlike
	0.65 ± 0.02	0.91 ± 0.01	OPAL [77]	2-jet	unlike
$\pi^\pm\pi^\pm$	$1.06 \pm 0.05 \pm 0.16$	$0.49 \pm 0.01 \pm 0.05$	DELPHI [30]	prompt pions	
$K^\pm K^\pm$	$0.82 \pm 0.11 \pm 0.25$	$0.48 \pm 0.04 \pm 0.07$	DELPHI [75]	all	unlike
	$0.82 \pm 0.22^{+0.17}_{-0.12}$	$0.56 \pm 0.08^{+0.08}_{-0.06}$	OPAL [76]	2-jet	mixed
$K^0_S K^0_S$	$1.14 \pm 0.23 \pm 0.32$	$0.76 \pm 0.10 \pm 0.11$	OPAL [78]	all	MC
	$0.61 \pm 0.16 \pm 0.16$	$0.55 \pm 0.08 \pm 0.12$	DELPHI [75]	all	MC
	$0.96 \pm 0.21 \pm 0.40$	$0.65 \pm 0.07 \pm 0.15$	ALEPH [79]	all	MC

4.4.2. The $K^0_S K^0_S$ system

The $K^0_S K^0_S$ system is a mixture of $K^0\bar{K}^0$ and K^0K^0 ($\bar{K}^0\bar{K}^0$) pairs. At LEPI energy, only 28% of all $K^0_S K^0_S$ pairs are estimated to come from the (identical) K^0K^0 or $\bar{K}^0\bar{K}^0$ system. What is particularly interesting is that K^0_S's can interfere even if they originate from a (non-identical) $K^0\bar{K}^0$ system [80]: An enhancement is expected in the low-Q region if one selects the $C = +1$ eigenstate of

$$|K^0\bar{K}^0>_{C=\pm1} = \frac{1}{\sqrt{2}}(|K^0(\boldsymbol{p})\bar{K}^0(-\boldsymbol{p})\rangle \pm \bar{K}^0(\boldsymbol{p})K^0(-\boldsymbol{p})\rangle), \qquad (39)$$

where $\boldsymbol{p}$ is the three-momentum of one of the kaons in their cms. In the limit $\boldsymbol{p} \to 0$ ($Q \to 0$), the $C = -1$ ($K^0_S K^0_L$) state disappears and $C = +1$ ($K^0_S K^0_S$ or $K^0_L K^0_L$) becomes maximal.

The enhancement in $K^0_S K^0_S$ and $K^0_L K^0_L$ pairs at low Q is exactly compensated by the low Q suppression of the $K^0_S K^0_L$ state, so that no BE effect is to be expected as long as all possible final states of the $K^0\bar{K}^0$ system are considered. A full BE-like enhancement is, however, expected for the $K^0_S K^0_S$ system by itself.

Early, low statistics results come from the hh experiment [81], new results exist from DELPHI [75,82], OPAL [78] and ALEPH [79]. While the kaon-production radius is smaller for the hh experiment, it seems to agree with those measured for both charged kaons and pions in the e^+e^- experiments, within the large spread of values observed. Furthermore, the parameter λ is large in agreement with the expectation [80].

4.4.3. $\Lambda^0\Lambda^0$ or $\bar{\Lambda}^0\bar{\Lambda}^0$

An interesting generalization of the Bose–Einstein formalism used above is to consider Fermi–Dirac interference, essentially by changing the sign in front of the correlator. This leads to a destructive interference at small phase-space distance and allows to determine the emission radius for identical fermions in a comparison of the amount of their total-spin $S = 1$ state (destructive) to that of their $S = 0$ state (constructive) as a function of Q [83]. The method does not need a further reference sample. It was applied to e^+e^- data at LEPI in [84–86] and gives a radius of about 0.15 fm. It was, however, verified, that the conventional method with JETSET as a reference sample gives similarly low a radius.

4.4.4. (Transverse) mass dependence of the radius parameter

The simultaneous comparison of the emission radii for pions, kaons and Λ's now suggests a decrease with increasing mass. Such a behavior has first been observed by NA44 in heavy-ion collisions [73]. The NA44 results can be translated into an $1/\sqrt{m}_{\mathrm{T}}$ scaling of the radius, in agreement with the expectations from a hydrodynamical model [70] with three-dimensional collective expansion and cylindrical symmetry.

In Fig. 10(a), the radius parameter r is shown as a function of the hadron mass m [88] for e^+e^- annihilation at the Z mass. The large error associated with $r_{\pi\pi}$ reflects the systematic uncertainty due to the choice of the reference sample. A general trend can be observed as a hierarchy

$$r_{\pi\pi} > r_{KK} > r_{\Lambda\Lambda}\,. \tag{40}$$

Some effect is to be expected from kinematics, *i.e.* from the mass-dependent integration limits when transforming from $R_2(\boldsymbol{p}_1, \boldsymbol{p}_2)$ in six-dimensional momentum space to $R_2(Q)$ in one-dimensional momentum separation [89]. This effect is far too small, however.

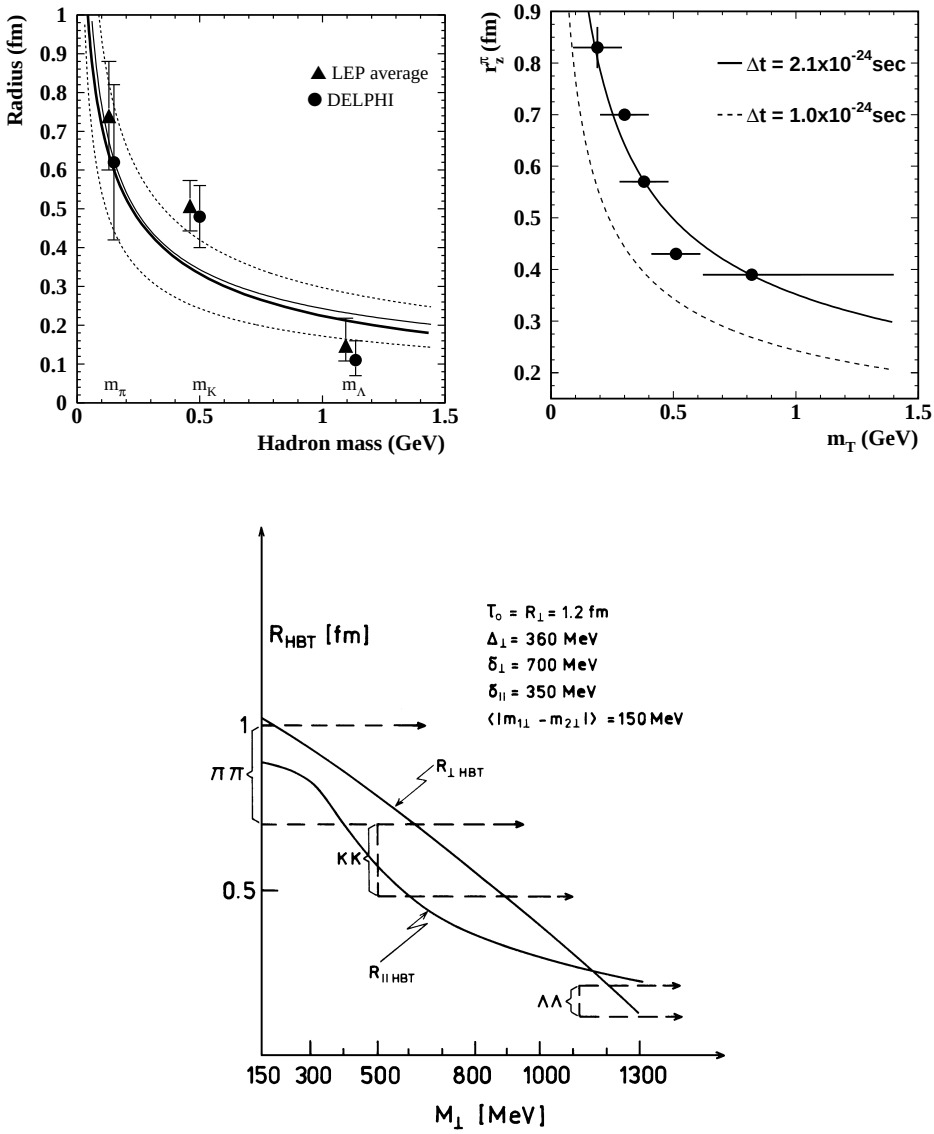


Fig. 10. (a) The radius parameter r as a function of the hadron mass m. (b) The longitudinal emitter radius r_z as a function of m_{T} [90]. The lines are described in the text [88]. (c) Longitudinal and transverse radius as a function of the transverse mass $M_\perp$ of the two-particle system, compared to the $M_\perp$-threshold values (same as data in Fig. 10(a)) [91].

The authors [88] show that a $1/\sqrt{m}$ behavior can be expected already from the Heisenberg principle with

$$\begin{aligned} \Delta p \Delta r &= mvr = \hbar c, \\ \Delta E \Delta t &= p^2 \Delta t / m = \hbar \end{aligned} \tag{41}$$

$$\text{and} \quad r = \frac{c\sqrt{\hbar \Delta t}}{\sqrt{m}}\,, \tag{42}$$

where m, v and p are the hadron mass, velocity and momentum and r is the distance between the two hadrons. Assuming ΔE to only depend on the kinetic energy of the produced particle and $\Delta t = 10^{-24}$ sec, independent of m, grants the thin solid line in Fig. 10(a). The upper and lower dashed lines correspond to an increase or decrease of Δt by $0,5 \cdot 10^{-24}$ sec, respectively. (The thick solid line corresponds to a perturbative QCD cascade using the virial theorem and assuming local parton hadron duality (LPHD).)

However, as shown in [88], a formula identical to (42) also holds for the radius r_{z} in the longitudinal direction and the average transverse mass $\bar{m}_{\mathrm{T}} = 0.5\,(\sqrt{m^2 + p_{\mathrm{T1}}^2} + \sqrt{m^2 + p_{\mathrm{T2}}^2})$. Fig. 10(b) shows DELPHI results [90] compared to $\Delta t = 10^{-24}$sec (dashed) and the best fitted value of $\Delta t = 2.1 \times 10^{-24}$sec (full line).

Alternatively, the transverse mass dependence can be explained by a generalized inside-outside cascade [91] assuming *(i)* approximate proportionality of four-momenta and production space–time position (freeze-out point) of the emitted particles $p_\mu = a x_\mu$ and *(ii)* a freeze-out time distributed along the hyperbola $\tau_0^2 = t^2 - z^2$ (*i.e.*, a generalization of the so-called Bjorken–Gottfried conditions). From the two conditions above follows directly

$$a^2 \tau_0^2 = E^2 - p_z^2 = m_{\mathrm{T}}^2 \tag{43}$$

and the generalized Bjorken–Gottfried condition

$$p_\mu = \frac{m_{\mathrm{T}}}{\tau_0} x_\mu\,. \tag{44}$$

Using a more rigorous formulation in terms of the Wigner representation, the authors show how this proportionality leads to an m_{T} dependence of the radius parameter. Fig. 10(c) gives indeed a dependence of both the longitudinal and the transverse radius on the transverse mass of the two-particle system,

$$M_\perp^2 = \bar{m}_{\mathrm{T}}^2 + m_{\mathrm{T1}} m_{\mathrm{T2}} \sinh^2\left(\frac{y_1 - y_2}{2}\right). \tag{45}$$

For a set of "reasonable" model parameters [91], the experimental results (same as in Fig. 10(a)) are reproduced reasonably well. Note that the experimental data are given at the threshold value of the corresponding $M_\perp$ at which transverse momenta and rapidity differences are small compared to the particle masses.

The parameters are to be improved, but $\Delta_\perp$ is closely related to the average transverse momentum and $\delta_\perp$ has to be considerably larger than $\Delta_\perp$ in the model to satisfy the uncertainty principle. Since $\delta_\perp$ corresponds to a correlation length between transverse momentum and transverse position at freeze-out, this correlation is rather weak. Nevertheless, it is sufficient to create a strong variation of the transverse radius, and suggests the existence of an important "collective flow", even in the system of particles produced in e^+e^- annihilation! Note that strong space–time momentum-space correlations are expected not only from hydrodynamic expansion but also from jet fragmentation.

4.5. The multiplicity (or density) dependence

In nucleus–nucleus experiments [92, 93], the radius r was found to increase with increasing charged-particle multiplicity n. By relating r to the size of the overlap region of the two colliding particles, this increase can be understood in terms of the geometrical model [94]: a large overlap should imply a large multiplicity. On the other hand, no evidence for a multiplicity dependence is found in hadron–nucleus collisions at 200 GeV/c [95].

After some time of confusion, the n dependence is now clear for hadron–hadron collisions. At energies below $\sqrt{s} \approx 30$ GeV (*i.e.* at $\sqrt{s} \approx 8$ [96], 22 [97] and 27 GeV [72]) no n-dependence is observed for $r_{\rm G}$. At higher energies (last Ref. [98] and [71]) an n-dependence starts to set in and to grow with increasing energy (see Fig. 11(a)). At the highest ISR energy ($\sqrt{s} = 62$ GeV) the increase is about 40% when the density in rapidity is doubled, but at $\sqrt{s} = 31$ GeV the increase is still very weak. The result is extended to $\sqrt{s} = 630$ GeV by UA1 [99] and to 1800 GeV by E735 [100] in Fig. 11(b). At very large density, the increase of $r_{\rm G}$ with increasing density is shown to extrapolate well to the heavy-ion results of NA35 [93] in Fig. 11(c). The effect is reproduced in thermodynamical and hydrodynamical models. The λ parameter, on the other hand, decreases with increasing n (not shown).

At the low-density side, the effect is also observed in e^+p collisions by H1 [60] (crosses in Fig. 11(b)). The results from e^+e^- experiments at lower energy [26,101] were consistent with no multiplicity dependence as expected from the geometrical model, but also for this type of collisions a multiplicity dependence was finally established at higher energy [77] (see Fig. 12(a)). At 91 GeV, the radius $r_{\rm G}$ is found to increase linearly with increasing multiplicity n, showing a small but statistically significant increase of about 10% for $10 \leq n \leq 40$. As for hh-collisions, the chaoticity parameter $\lambda_{\rm G}$ decreases with increasing n.

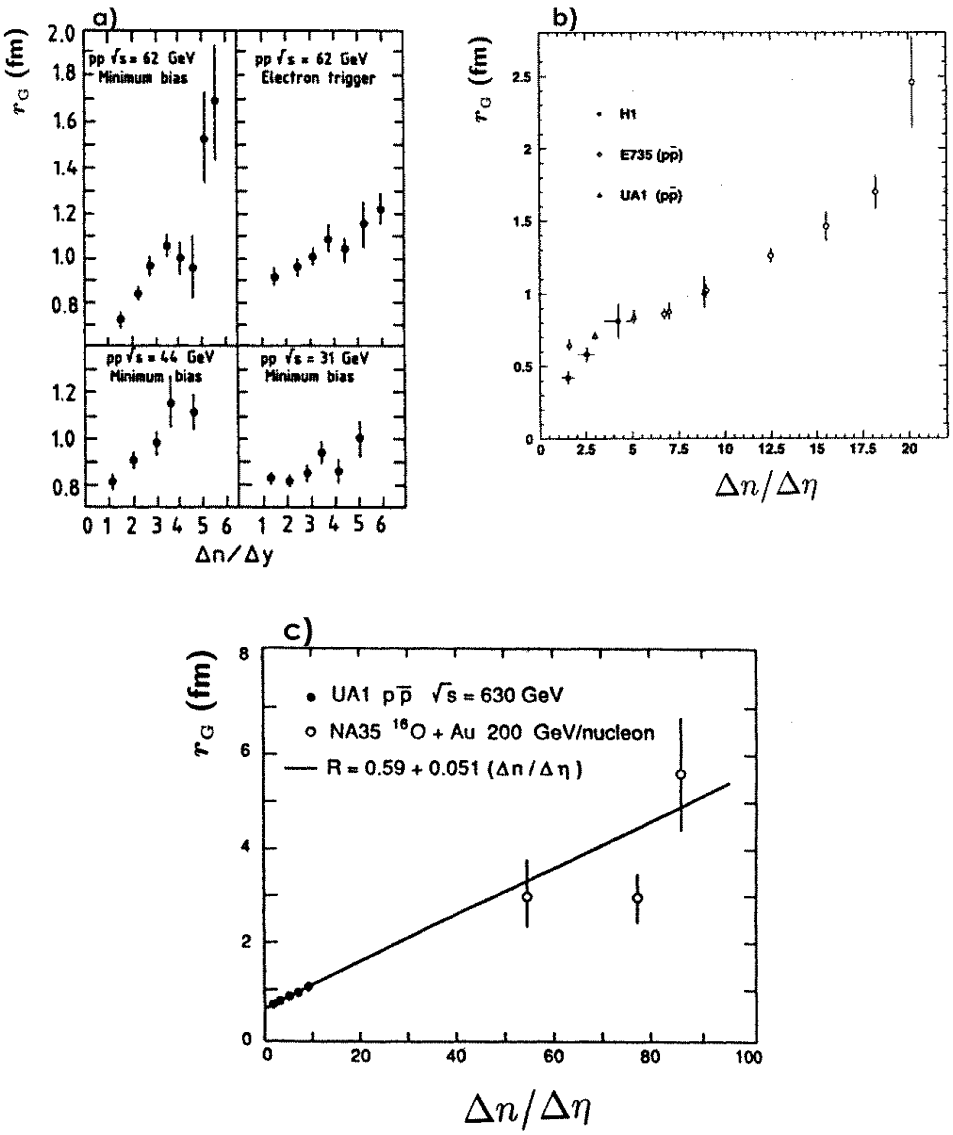


Fig. 11. (a) Radius r_G of the pion source as a function of charged-particle density for the energies indicated [98], b) same for $p\bar{p}$ collisions at 630 GeV [99] and 1800 GeV [100], as well as e^+p collisions at 300 GeV [60], c) Comparison of r_G as a function of charged-particle density $\Delta n/\Delta\eta$ [99] with the results of relativistic heavy-ion collisions [93].

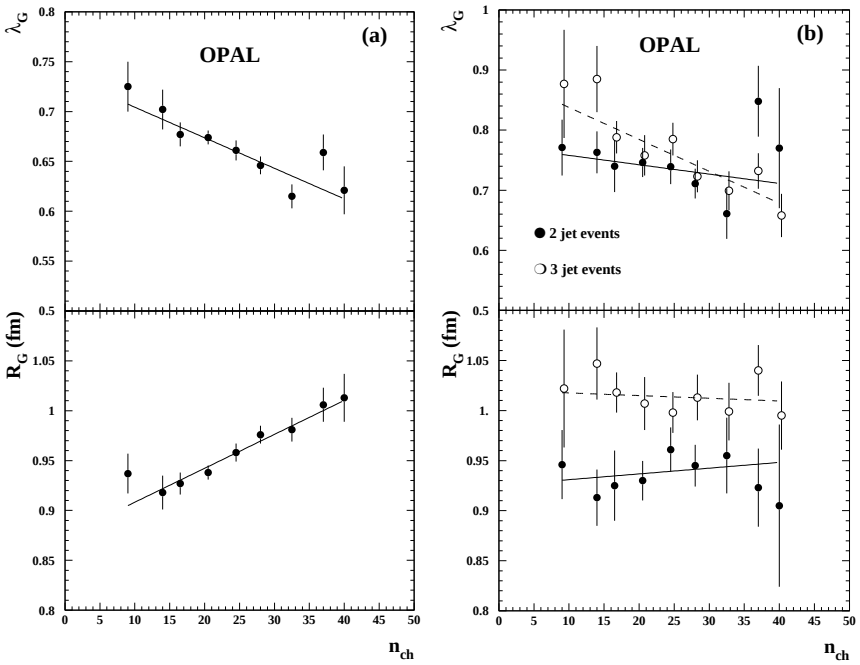


Fig. 12. (a) Dependence of λ_G and r_G on the charged-particle multiplicity n for e^+e^- collisions at the Z mass, (b) same for two-jet events (solid points) and three-jet events (open points) [77].

In Fig. 12(b), OPAL further shows that the multiplicity dependence is strongly reduced in separate samples of two-jet and three-jet events, the average value of r_G, however, being 10% bigger for three-jet than for two-jet events. Folding in the multiplicity difference of two- and three-jet events, this at least partly explains the effect as due to multi-jet production at higher energies. The decrease of λ is larger in the 3-jet than in the 2-jet sample.

As shown quantitatively in [102], it is crucial to study the normalized cumulants $K_2(Q)$ (Eq. (11)) rather than the normalized densities $R_2(Q)$ (Eq. (10)) in a density dependent analysis and to correct for a well-defined multiplicity-dependent bias due to the cut in the multiplicity distribution (the point being that $K_q \neq 0$ for limited n, even in case of independent emission). In Fig. 13(a) and (b) [103], the bias-corrected (so-called "internal") cumulants are given for UA1 as a function of the inverse rapidity density, for small and large values of Q, respectively. The data show

(i) a linear dependence (similar for like-charged and unlike-charged pairs),
(ii) vanishing of the cumulant at large density for large Q,
(iii) approach towards a finite limit for large density at small Q (where BE correlations are expected to dominate).

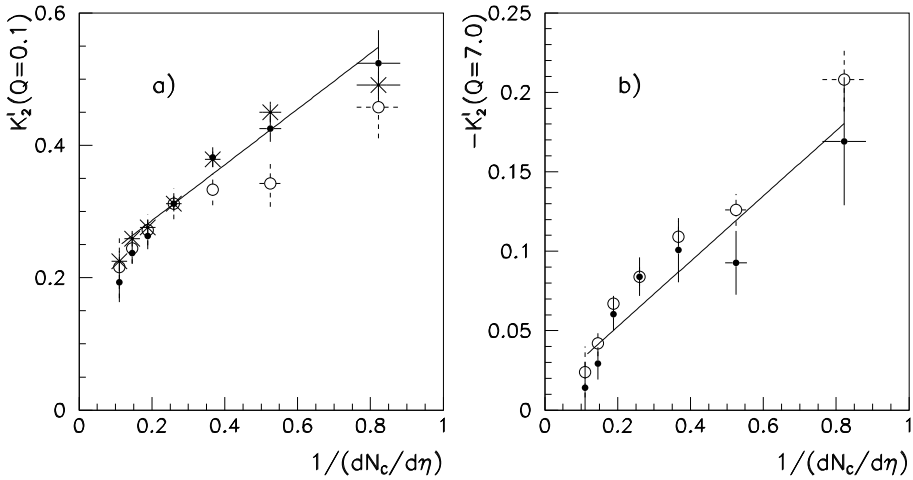


Fig. 13. Inverse density dependence of the bias-corrected cumulant at $Q = 0.1$ GeV (a) and $Q = 7.0$ GeV (b) for like-charged pairs (full circles) and unlike-charged pairs (open circles). The crosses in (a) correspond to λ-values [103].

The large-Q behavior [points *(i)* and *(ii)* above] is that expected from particle emission from N fully overlapping, identical but fully independent sources (*e.g.* strings). From the additivity of unnormalized cumulants follows immediately a dilution,

$$K_q^{(N)}(y_1,\ldots,y_q) = \frac{NC_q(y_1,\ldots,y_q)}{N^q C_1^q(y_1,\ldots,y_q)} = \frac{1}{N^{(q-1)}} K_q^{(1)}(y_1,\ldots,y_q)\ , \qquad (46)$$

where $K_q^{(N)}$ is the normalized cumulant of the N-source system, while $K_q^{(1)}$ is that of an individual source (see also [104–106]). This results in a normalized cumulant inversely proportional to N or to the total density $dn/dy = Ndn^{(1)}/dy$, as observed in Fig. 13(b).

At small Q (Fig. 13(a)), however, the normalized cumulant approaches a constant different from zero at large densities. Naively, this would imply correlations between particles coming from different sources, which could be interpreted as inter-source Bose–Einstein correlations, would not a similar effect be observed for unlike-charged pairs, as well. So also resonances play an important part. One has to keep in mind, however, that (46) only holds for full overlap of identical sources and that at $Q \approx 0.1$ GeV the overlap is far from complete and the number of sources limited.

However, also in heavy-ion collisions there is evidence that λ does not drop with increasing density for ever. Heavy-ion collisions lead to λ values quickly decreasing with increasing density at lower densities (*i.e.* lower-A collisions). In agreement with the expectation for overlapping independent sources, λ drops from 0.79 to 0.32 [107] from O–C to O–Cu, O–Ag and O–Au. In high-A collisions, on the other hand, a saturation seems to set in [108,109]. For S–Pb and Pb–Pb central collisions NA44 [73] quotes $\lambda = 0.56$ and 0.59, respectively. Such a saturation and eventual increase of λ would be expected if the densely packed strings of a heavy-ion collision finally coalesce until they form a large single fireball (percolation of strings) [109].

4.6. The emission function

As has become clear from the previous sub-sections, the correlation measurements alone do not contain the complete information on the geometrical and dynamical parameters characterizing the evolution of the hadronic matter. In particular, BEC are not measuring the full geometrical size of large and expanding systems, since that expansion results in strong correlations between space–time and momentum space. More comprehensive information can be provided by a combined analysis of data on two-particle correlations and single-particle inclusive spectra [21,87,110–112].

4.6.1. The formalism

In the framework of the hydrodynamical model for three-dimensionally expanding cylindrically-symmetric systems [87], the emission function corresponds to a Boltzmann approximation of the local momentum distribution. Within this model, the invariant single-particle spectrum of pions in rapidity y and transverse mass m_{T} is approximated by

$$\begin{aligned} f(y, m_{\mathrm{T}}) &= \frac{1}{N_{\mathrm{ev}}} \frac{dN_\pi}{dy dm_{\mathrm{T}}^2} \\ &= C {m_{\mathrm{T}}}^{\alpha} \cosh\eta_s \exp\left(\frac{\Delta\eta_*^2}{2}\right) \exp\left[-\frac{(y-y_0)^2}{2\Delta y^2}\right] \exp\left(-\frac{m_{\mathrm{T}}}{T_0}\right) \\ &\quad \times \exp\left\{\frac{\langle u_{\mathrm{T}}\rangle^2 (m_{\mathrm{T}}^2 - m_\pi^2)}{2T_0[T_0 + (\langle u_{\mathrm{T}}\rangle^2 + \langle \frac{\Delta T}{T}\rangle) m_{\mathrm{T}}]}\right\}. \end{aligned} \tag{47}$$

with

$$\Delta y^2 = \Delta\eta^2 + \frac{T_0}{m_{\mathrm{T}}}, \tag{48}$$

$$\frac{1}{\Delta\eta_*^2} = \frac{1}{\Delta\eta^2} + \frac{m_{\mathrm{T}}}{T_0}\cosh\eta_{\mathrm{s}}, \tag{49}$$

$$\eta_{\rm s} \;=\; \frac{y-y_0}{1+\Delta\eta^2\,\frac{m_{\rm T}}{T_0}}\,. \tag{50}$$

The width Δy of the rapidity distribution given by (48) is determined by the width $\Delta\eta$ of the longitudinal space–time rapidity η distribution of the pion emitters and by the thermal smearing width $\sqrt{T_0/m_{\rm T}}$, where T_0 is the freeze-out temperature (at the mean freeze-out time $\tau_{\rm f}$) at the axis of the hydrodynamical tube, $T_0 = T_{\rm f}(r_{\rm T}=0)$. For the case of a slowly expanding system one expects $\Delta\eta \ll T_0/m_{\rm T}$, while for the case of a relativistic longitudinal expansion the geometrical extension $\Delta\eta$ can be much larger than the thermal smearing (provided $m_{\rm T} > T_0$).

Except for the inhomogeneity caused by the longitudinal expansion, (47) also considers the inhomogeneity related to the transverse expansion (with the mean radial component $\langle u_{\rm T}\rangle$ of hydrodynamical four-velocity) and to the transverse temperature inhomogeneity, characterized by the quantity

$$\left\langle \frac{\Delta T}{T} \right\rangle = \frac{T_0}{T_{\rm rms}} - 1\,, \tag{51}$$

where $T_{\rm rms} = T_{\rm f}(r_{\rm T} = r_{\rm T}({\rm rms}))$ is the freeze-out temperature at the transverse rms radius $r_{\rm T}({\rm rms})$ and at time $\tau_{\rm f}$.

The power α in (47) is related [87] to the number d of dimensions in which the expanding system is inhomogeneous. For the special case of the one-dimensional inhomogeneity ($d=1$) caused by the longitudinal expansion, $\alpha = 1 - 0.5d = 0.5$ (provided $\Delta\eta^2 \gg T_0/m_{\rm T}$). The transverse inhomogeneity of the system leads to smaller values of α. The minimum value of $\alpha = -1$ is achieved at $d=4$ for the special case of a three-dimensionally expanding system with temporal change of local temperature during the particle emission process.

The parameter y_0 in (47) denotes the midrapidity in the interaction c.m.s. and can slightly differ from 0 due to different species of colliding particles. The parameter C is an overall normalization coefficient.

Note that (47) yields the single-particle spectra of the core (the central part of the interaction that supposedly undergoes collective expansion). However, also long-lived resonances contribute to the single-particle spectra through their decay products. Their contribution can be determined in the core-halo picture [70,113] by the momentum dependence of the strength parameter $\lambda(y, m_{\rm T})$ of the two-particle Bose–Einstein correlation function. Experimentally, the parameter is however found to be approximately independent of $m_{\rm T}$ [114–116]. Hence this correction can be absorbed in the overall normalization.

The two-dimensional distribution (47) can be simplified for one-dimensional slices [38,87,116]:

1. At fixed m_{T}, the rapidity distribution reduces to the approximate parametrization

$$f(y, m_{\mathrm{T}}) = C_m \exp\left[-\frac{(y-y_0)^2}{2\Delta y^2}\right], \tag{52}$$

where C_m is an m_{T}-dependent normalization coefficient and y_0 is defined above. The width parameter Δy^2 extracted for different m_{T}-slices is predicted to depend linearly on $1/m_{\mathrm{T}}$, with slope T_0 and intercept $\Delta\eta^2$ (*cf.* (48)).

Note, that for static fireballs or spherically expanding shells (52) and (48) are satisfied with $\Delta\eta = 0$ [38]. Hence, the experimental determination of the $1/m_{\mathrm{T}}$ dependence of the Δy parameter can be utilized to distinguish between longitudinally expanding finite systems versus static fireballs or spherically expanding shells.

2. At fixed y, the m_{T}^2-distribution reduces to the approximate parametrization

$$f(y, m_{\mathrm{T}}) = C_y m_{\mathrm{T}}^{\alpha} \exp\left(-\frac{m_{\mathrm{T}}}{T_{\mathrm{eff}}}\right), \tag{53}$$

where C_y is a y-dependent normalization coefficient and α is defined as above.

The y-dependent "effective temperature" $T_{\mathrm{eff}}(y)$ can be approximated as

$$T_{\mathrm{eff}}(y) = \frac{T_*}{1 + a(y-y_0)^2}, \tag{54}$$

where T_* is the maximum of $T_{\mathrm{eff}}(y)$ achieved at $y = y_0$, and

$$a = \frac{T_0 T_*}{2m_\pi^2(\Delta\eta^2 + \frac{T_0}{m_\pi})^2} \tag{55}$$

with T_0 and $\Delta\eta^2$ as defined above.

The approximations (52) and (53) explicitly predict a specific narrowing of the rapidity and transverse mass spectra with increasing m_{T} and y, respectively (*cf.* (48) and (54)). The character of these variations is expected [38] to be different for the various scenarios of hadron matter evolution.

4.6.2. The results

The Δy^2 values obtained from fits of the NA22 data [116] by (52) are given as a function of $1/m_{\mathrm{T}}$ in Fig. 14(a). A fit to the widening of the rapidity distribution (*i.e.* increase of Δy^2) with increasing $1/m_{\mathrm{T}}$ by (48) gives an

intercept $\Delta\eta^2 = 1.91 \pm 0.12$ and slope $T_0 = 159 \pm 38$ MeV. Thus, the width of the y-distribution is dominated by the spatial (longitudinal) distribution of pion emitters (inherent to longitudinally expanding systems) and not by the thermal properties of the hadron matter, as would be expected for static or radially expanding sources. Since $\Delta\eta^2$ is significantly bigger than 0, static fireballs or spherically expanding shells, able to describe the two-particle correlation data in [115], fail to reproduce the single-particle spectra.

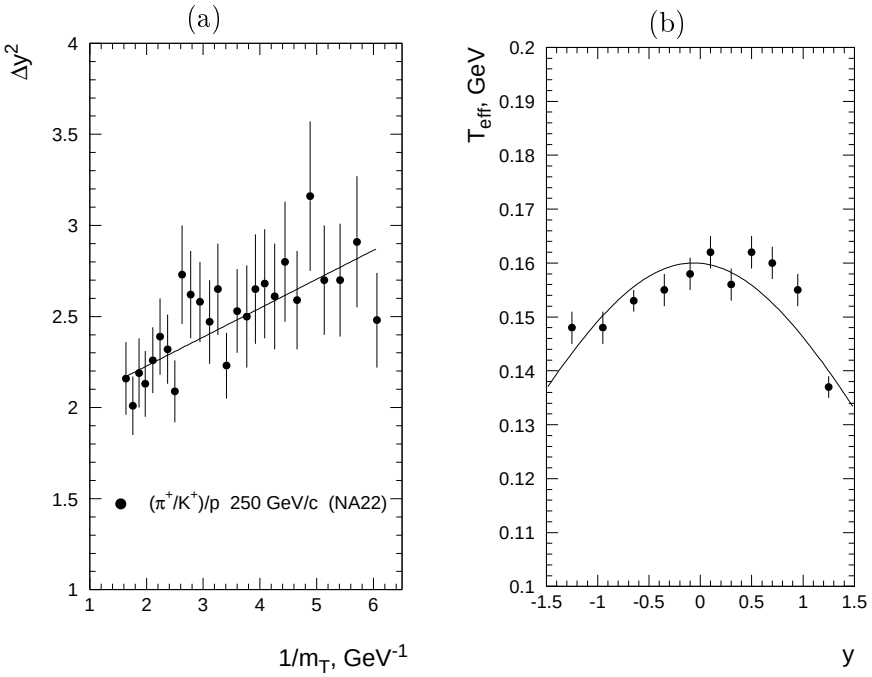


Fig. 14. (a) The $(1/m_{\mathrm{T}})$-dependence of $(\Delta y)^2$ for inclusive π^- meson rapidity distributions at $|y| < 1.5$. The straight line is the fit result according to parametrization (48). (b) T_{eff} as a function of y fitted according to parametrization (54) [116].

The T_{eff} values obtained from fits of the same data by (53) are given as a function of y in Fig. 14(b). $T_{\mathrm{eff}}(y)$ tends to decrease with increasing $|y|$ and approximately follows (54) with $T_* = 160 \pm 1$ MeV, $a = 0.083 \pm 0.007$ and $y_0 = -0.065 \pm 0.039$. Note, however, an asymmetry in the T_{eff} distribution with respect to $y = 0$: except for the last point, T_{eff} is higher in the meson than in the proton hemisphere.

The values of the exponential parameter α fitted in (53) are near zero, corresponding to a two-dimensional inhomogeneity of the expanding system ($\alpha = 1 - 0.5d$). One concludes, therefore, that apart from a longitudinal inhomogeneity caused by the relativistic longitudinal flow, the hadron matter

also has a transverse inhomogeneity (caused by transverse expansion or a transverse temperature gradient) or undergoes a temporal change of local temperature during the particle emission process.

4.6.3. The transverse direction

Further information on hadron–matter evolution in the transverse direction can be extracted from (47) with parameters $\langle u_{\mathrm{T}} \rangle$ and $\langle \frac{\Delta T}{T} \rangle$ characterizing the strength of the transverse expansion and temperature inhomogeneity.

A moderate value of the mean transverse four-velocity $\langle u_{\mathrm{T}} \rangle = 0.20 \pm 0.07$ indicates that the transverse inhomogeneity is mainly stipulated by the rather large temperature inhomogeneity $\langle \frac{\Delta T}{T} \rangle = 0.71 \pm 0.14$. Using (51), one infers that the freeze-out temperature decreases from $T_0 = 140 \pm 3$ MeV at the central axis of the hydrodynamical tube to $T_{\mathrm{rms}} = 82 \pm 7$ MeV at a radial distance equal to the transverse rms radius of the tube.

4.6.4. Combination with two-particle correlations

Due to the non-static nature of the source, the effective size parameters $r_{\mathrm{L}}, r_{\mathrm{out}}, r_{\mathrm{side}}$ vary with the average transverse mass $\bar{m}_{\mathrm{T}} = \frac{1}{2}(m_{\mathrm{T}1} + m_{\mathrm{T}2})$ and the average rapidity $Y = \frac{1}{2}(y_1 + y_2)$ of the pion pair. In the LCMS the effective radii can be approximated [38, 87, 111] by

$$r_{\mathrm{L}}^2 = \tau_{\mathrm{f}}^2 \Delta\eta_*^2 \,, \tag{56}$$

$$r_{\mathrm{out}}^2 = r_*^2 + \beta_{\mathrm{T}}^2 \Delta\tau_*^2 \,, \tag{57}$$

$$r_{\mathrm{side}}^2 = r_*^2 \tag{58}$$

with

$$\frac{1}{\Delta\eta_*^2} = \frac{1}{\Delta\eta^2} + \frac{\bar{m}_{\mathrm{T}}}{T_0} \,, \tag{59}$$

$$r_*^2 = \frac{r_g^2}{1 + \frac{\bar{m}_{\mathrm{T}}}{T_0}(\langle u_{\mathrm{T}} \rangle^2 + \langle \frac{\Delta T}{T} \rangle)} \,, \tag{60}$$

where the parameters $\Delta\eta^2, T_0, \langle u_{\mathrm{T}} \rangle$ and $\langle \frac{\Delta T}{T} \rangle$ are defined and estimated from the invariant spectra above; r_g is related to the transverse geometrical rms radius of the source as $r_g(\mathrm{rms}) = \sqrt{2} r_g$; τ_{f} is the mean freeze-out (hadronization) time; $\Delta\tau_*$ is related to the duration $\Delta\tau_{\mathrm{f}}$ of pion emission and to the temporal inhomogeneity of the local temperature. If the latter has a small strength (as one can deduce from the restricted inhomogeneity dimension estimated above), an approximate relation $\Delta\tau_{\mathrm{f}} \geq \Delta\tau_*$ holds. The variable β_{T} is the transverse velocity of the pion pair.

Using (56) and (59) with $T_0 = 140 \pm 3$ MeV and $\Delta\eta^2 = 1.85 \pm 0.04$, together with $r_{\rm L}$ fitted in different $\bar{m}_{\rm T}$ ranges, one finds a mean freeze-out time of $\tau_{\rm f} = 1.4 \pm 0.1$ fm/c.

The transverse-plane radii $r_{\rm out}$ and $r_{\rm side}$ measured in [115] for the whole $\bar{m}_{\rm T}$ range are: $r_{\rm out} = 0.91 \pm 0.08$ fm and $r_{\rm side} = 0.54 \pm 0.07$ fm. Substituting into (57) and (58), one obtains (at $\beta_{\rm T} = 0.484c$ [115]): $\Delta\tau_* = 1.3 \pm 0.3$ fm/c. Since the mean duration time of pion emission can be estimated as $\Delta\tau_{\rm f} \geq \Delta\tau_*$, the data grant $\Delta\tau_{\rm f} \approx \tau_{\rm f}$. A possible interpretation is that in meson-proton collisions the radiation process occurs during almost all the hydrodynamical evolution of the hadronic matter produced.

An estimation for the parameter r_g can be obtained from (58) and (60) using the quoted values of $r_{\rm side}, T_0, \langle u_{\rm T}\rangle$ and $\langle\frac{\Delta T}{T}\rangle$. The geometrical rms transverse radius of the hydrodynamical tube, $r_g({\rm rms}) = \sqrt{2} r_g = 1.2 \pm 0.2$ fm, turns out to be larger than the proton rms transverse radius.

The set of parameters of the combined analysis of single-particle spectra and Bose–Einstein correlations in $(\pi^+/{\rm K}^+)p$ collisions [116] is compared to that obtained [117] from averaging over Pb+Pb experiments (NA49, NA44 and WA98) in Table III.

TABLE III

Fit parameters of the Buda–Lund Hydro (B–LH) model in a combined analysis of NA22 [116], NA49, NA44, WA98 [117] spectra and correlation data.

Param.	NA22	Heavy ion averaged
T_0 [MeV]	140 ± 3	139 ± 6
$\langle u_{\rm T}\rangle$	0.20 ± 0.07	0.55 ± 0.06
r_g [fm]	1.2 ± 0.2	7.1 ± 0.2
$\tau_{\rm f}$ [fm/c]	1.4 ± 0.1	5.9 ± 0.6
$\Delta\tau_{\rm f}$ [fm/c]	1.3 ± 0.3	1.6 ± 1.5
$\Delta\eta$	1.36 ± 0.02	2.1 ± 0.4
$\langle\frac{\Delta T}{T}\rangle$	0.71 ± 0.14	0.06 ± 0.05
y_0	0.082 ± 0.006	0 (fixed)

The temperature T_0 near 140 MeV comes out surprisingly similar for hh and PbPb collisions. The geometrical radius r_g and the mean freeze-out time τ_f are of course larger for PbPb than for hh collisions, but surprising is the similarity of the duration $\Delta\tau_\mathrm{f}$ of emission in both. The fact that $\Delta\tau_\mathrm{f} \approx \tau_\mathrm{f}$ in hh collisions, indicates that the radiation process occurs during all the evolution of hadronic matter in this type of collisions. On the other hand, $\Delta\tau_\mathrm{f} < \tau_\mathrm{f}$ for PbPb collisions suggests that there the radiation process only sets in at the end of the evolution. Other important differences are the large transverse flow velocity $\langle u_\mathrm{T}\rangle$ and small transverse temperature gradient in PbPb as compared to hh collisions.

4.6.5. The space–time distribution of π emission

Figure 15(a) gives a reconstruction of the space–time distribution of pion emission points [116], expressed as a function of the cms time variable t and the cms longitudinal coordinate z. The momentum-integrated emission function along the z-axis, *i.e.*, at $(x, y) = (0, 0)$ is given by

$$S(t,z) \propto \exp\left(-\frac{(\tau-\tau_\mathrm{f})^2}{2\Delta\tau_\mathrm{f}^2}\right)\exp\left(-\frac{(\eta-y_0)^2}{2\Delta\eta^2}\right) . \tag{61}$$

It relates the parameters fitted to the NA22 data with particle production in space–time. Note that the coordinates (t, z), can be expressed with the help of the longitudinal proper-time τ and space–time rapidity η as $(\tau\cosh\eta, \tau\sinh\eta)$.

One finds a structure resembling a boomerang, *i.e.*, particle production takes place close to the regions of $z = t$ and $z = -t$, with gradually decreasing probability for ever larger values of space–time rapidity. Although the mean proper-time for particle production is $\tau_\mathrm{f} = 1.4\,\mathrm{fm}/c$, and the dispersion of particle production in space–time rapidity is rather small ($\Delta\eta = 1.36$), a characteristic long tail of particle emission is observed on both sides of the light-cone, giving more than 40 fm longitudinal extension in z and 20 fm/c duration of particle production in the time variable t.

An, at first sight, similar behavior is seen in Fig. 15(c) for PbPb collisions [117]. An important quantitative difference is, however, that particle emission starts immediately in hadron–hadron collision, but only after about 4–5 fm/c in PbPb collisions!

The information on $\langle u_\mathrm{T}\rangle$ and $\langle\frac{\Delta T}{T}\rangle$ from the analysis of the transverse momentum distribution can be used to reconstruct the details of the transverse density profile. An exact, non-relativistic hydro solution was found [119] using an ideal gas equation of state. In this hydro solution, both

$$\left\langle\frac{\Delta T}{T}\right\rangle \geqslant \frac{m\langle u_\mathrm{T}\rangle^2}{T_0} , \tag{62}$$

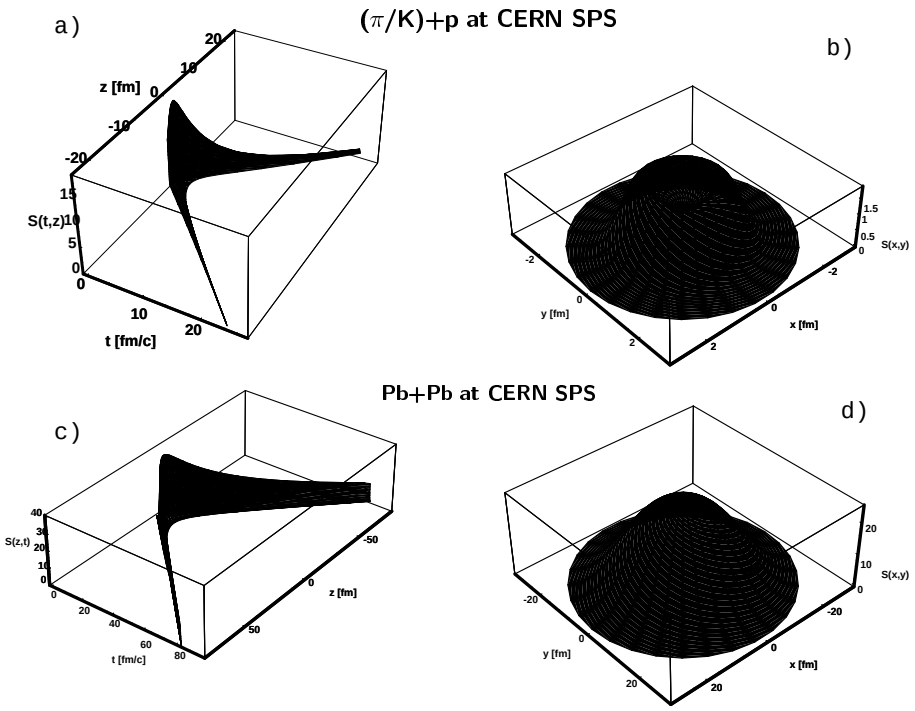


Fig. 15. The reconstructed emission function $S(t,z)$ in arbitrary vertical units, as a function of time t and longitudinal coordinate z (left diagrams), as well as the reconstructed emission function $S(x,y)$ in arbitrary vertical units, as a function of the transverse coordinates x and y (right pictures), for hh (upper pictures) and PbPb (lower pictures) collisions, respectively [116–118].

are possible. The $<$ sign corresponds to a self-similar expanding fire-ball, while the $>$ sign corresponds to a self-similar expanding ring of fire (see Fig. 16).

Assuming the validity of this non-relativistic solution, one can reconstruct the detailed shape of the transverse density profile. The result looks like a ring of fire in the x,y plane in hh interactions (Fig. 15(b)), while in PbPb collisions it has a Gaussian shape (Fig. 15(d)).

The formation of a ring of fire in hh collisions is due to the rather small transverse flow and the sudden drop of the temperature in the transverse direction, which leads to large pressure gradients in the center and small pressure gradients and a density augmentation at the expanding radius of the fire-ring. This transverse distribution, together with the scaling longitudinal expansion, creates an elongated, tube-like source in three dimensions, with the density of particle production being maximal on the surface of the tube.

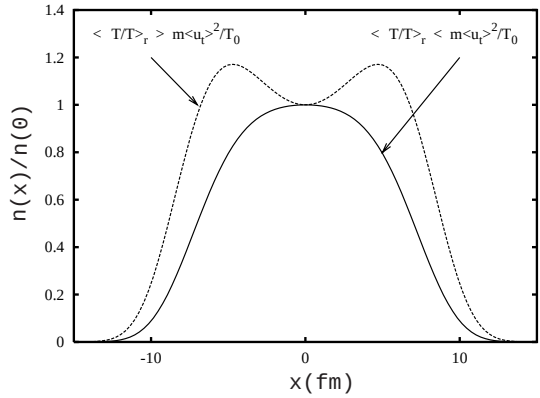


Fig. 16. Illustration of the development of smoke-ring solutions for large temperature gradients in exact solutions of non-relativistic hydrodynamics [119].

The pion emission function $S(x,y)$ for PbPb collisions, on the other hand, corresponds to the radial expansion, which is a well established phenomenon in heavy-ion collisions from low-energy to high-energy reactions. This transverse distribution, together with the scaling longitudinal expansion, creates a cylindrically symmetric, large and transversally homogeneous fireball, expanding three-dimensionally with a large mean radial component $\langle u_{\mathrm{T}} \rangle$ of hydrodynamical four-velocity.

Because of this large difference observed for those two types of collision, analysis of the emission function in e^+e^- collisions is of crucial importance for the understanding of the actual WW overlap and has been started.

4.7. The $\pi^0\pi^0$ system

In a string model, unlike $\pi^{\pm}\pi^{\pm}$-pairs, pairs of prompt π^0's can be emitted in adjacent string break-ups. In momentum space, the correlation function is, therefore, expected to be wider for neutral pions than for charged ones. Neutral pions, furthermore, do not suffer from Coulomb repulsion. However, the detection of several π^0's in one event requires high efficiency of γ-detection in a wide energy range and geometrical acceptance. Furthermore, the correlation function at small Q is strongly influenced by resonance decays as $\eta \to \pi^0\pi^0\pi^0$, $\eta' \to \pi^0\pi^0\eta$, $K^0_{\mathrm{S}}, f_0 \to \pi^0\pi^0$ and other final-state interactions [120].

First evidence for Bose–Einstein correlations in $\pi^0\pi^0$ pairs was found in [121]. In a first measurement of the radius in π^-Xe interactions at 3.5 GeV [122], the size of the π^0 emission region was found compatible with that for charged pions.

The question was taken up again by L3 [123], where both $r_{\rm G}$ and λ are found to be on the low side when compared to the $\pi^{\pm}\pi^{\pm}$ results obtained under the same experimental conditions. The difference in λ can at least partially be explained by the contribution of resonances. The difference in size parameter is $r_{\pm\pm} - r_{00} = 0.150 \pm 0.075 \pm 0.068$ fm.

4.8. Higher-order Bose–Einstein correlations

4.8.1. The formalism

It is convenient to use the normalized inclusive density and correlation functions already defined in Eqs.(10) and (11). The normalized inclusive density for two identical pions is

$$R_2(1,2) = 1 + K_2(1,2)\,. \tag{63}$$

In the limit of a completely chaotic and static pion source, $K_2(1,2)$ reduces to the square of the Fourier transform $F(\boldsymbol{p}_1 - \boldsymbol{p}_2, E_1 - E_2)$ of the space–time distribution of the source, $K_2(1,2) = |F(1,2)|^2$, where $\boldsymbol{p}_i$ and E_i $(i = 1,2)$ are the three-momentum and energy of pion i, respectively.

If the Gaussian parametrization is used for $|F(Q_2^2)|^2$, then one has

$$K_2(Q_2^2) = |F(Q_2^2)|^2 = \exp(-r_{\rm G}^2 Q_2^2)\,. \tag{64}$$

In terms of the Q_{ij} variables and for the case of a completely chaotic source, the normalized inclusive three-pion density is [124, 125]

$$\begin{aligned} R_3(1,2,3) \;=\; & 1 + |F(Q_{12}^2)|^2 + |F(Q_{23}^2)|^2 + |F(Q_{31}^2)|^2 \\ & + 2\mathrm{Re}\{F(Q_{12}^2)F(Q_{23}^2)F(Q_{31}^2)\}\,, \end{aligned} \tag{65}$$

so that the genuine three-particle correlation reads

$$K_3(1,2,3) = 2\mathrm{Re}\{F(Q_{12}^2)F(Q_{23}^2)F(Q_{31}^2)\}\,. \tag{66}$$

In general, the genuine three-particle correlation $K_3(1,2,3)$ is not expressed completely in terms of the two-particle correlation function (64), but contains also new information on the phase ϕ_{ij} of the Fourier transform of the source,

$$\cos\phi = \frac{K_3(1,2,3)}{2\sqrt{K_2(1,2)K_2(2,3)K_2(3,1)}}\,, \tag{67}$$

with $\phi \equiv \phi_{12} + \phi_{23} + \phi_{31}$ being a function of Q_{ij} and $\cos\phi \to 1$ as $Q_{ij} \to 0$. Geometrical asymmetry in the production mechanism (emission function) due to flow or resonance decays will only lead to small (few percent) reduction of $\cos\phi$ from unity [126]. Equation (67) is not valid for (partially)

coherent sources and more complicated expressions are needed [126]. If $\cos\phi$ considerably differs from unity at $Q_{ij} > 0$, one can infer that partial coherence is present (or, alternatively, that K_3 is suppressed due to dilution in the case of many independent sources!).

To the extent that phase factors may be neglected and the Gaussian approximation would hold, K_3 is related to K_2 via the expression

$$K_3(Q_3^2) = 2\exp(-\frac{r^2}{2}Q_3^2) = 2\sqrt{K_2(Q_3^2)} \tag{68}$$

with

$$Q_3^2 \equiv Q_{123}^2 = (P_1 + P_2 + P_3)^2 - 9M_\pi^2 = Q_{12}^2 + Q_{13}^2 + Q_{23}^2\,. \tag{69}$$

4.8.2. Genuine three-particle correlations

Non-zero genuine correlations up to order $q = 5$ were first established by the NA22 collaboration [127] in terms of cumulant moments. So they must show up here, as well. The function $K_3(Q_3^2) + 1$ is given in Fig. 17(a). A non-zero K_3 is indeed observed in the data for $Q_{3\pi}^2 < 0.2$ $(\mathrm{GeV}/c)^2$ [61], but not in FRITIOF.

Both observations, the existence of genuine three-particle correlations and the underestimate in JETSET are supported by DELPHI [128]. In Fig. 17(b), the three-particle correlation function $K_3 + 1$ is shown for like-charged triplets (upper) and unlike-charged triplets (lower), respectively, together with the prediction of JETSET with and without BE correlations. The parameters used to include the BE correlations are the same as in the two-particle correlation study of DELPHI [30]. The model is in reasonable agreement with the data for the $(++-)$ and $(+--)$ configurations but underestimates the enhancement for the $(+++)$ and $(---)$ correlations. Bose–Einstein interference in JETSET not only changes the distribution of like-sign correlations, but also the unlike-sign ones and leads to better agreement with the data.

Statistically a better evidence for genuine three-particle BE correlations now comes from OPAL [129]. This is shown in Fig. 17(c), together with a Gaussian fit over the range $0.25 < Q_3 < 2.0$ GeV, giving $r_3 = 0.580 \pm 0.004 \pm 0.025$ fm and $\lambda_3 = 0.504 \pm 0.010 \pm 0.041$. Within two standard deviations, the value for r_3 agrees with the relation $r_3 = r_2/\sqrt{2}$ (see (68)) when compared to r_2 obtained in [77].

The question is, whether the observed genuine three-particle correlation can be fully expressed in terms of the simple product of two-particle correlation functions according to (68), or whether information can be extracted on the relative phases of (66). If relation (68) holds, the function $1+K_3(Q_3^2)$

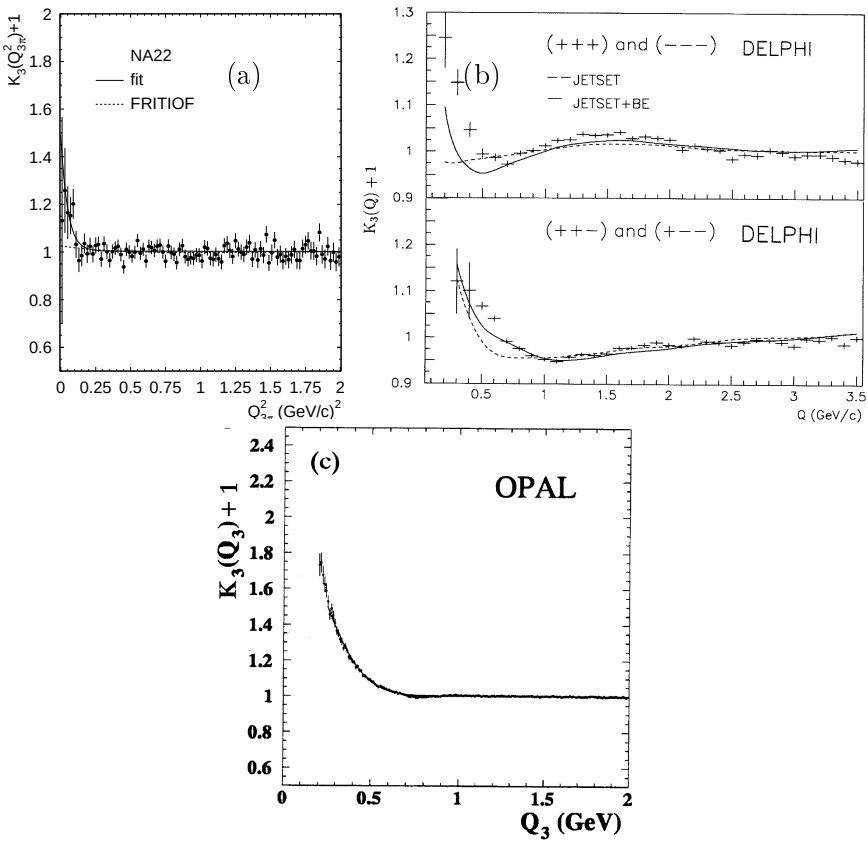


Fig. 17. (a) The normalized three particle correlation function $K_3(Q_3^2)$ added to 1. The full line is the result of a fit by (70), the dashed line corresponds to FRITIOF results [61]. (b) The function $K_3(Q)+1$ for like-sign triplets and unlike-sign triplets. The predictions of JETSET without BE (dashed line) and with BE correlations (full line) are also shown [128]. (c) Like-sign triplets after Coulomb correction, with a Gaussian fit (solid line) [129].

can be described by the parameters $r_2 = 0.85 \pm 0.01$ fm and $\lambda_2 = 0.38 \pm 0.02$ deduced from the fit of the normalized two-particle density $R_2(Q_2^2)$:

$$K_3(Q_3^2) + 1 = \gamma[1 + 2\lambda_2^{3/2} \exp(-\tfrac{1}{2} r_2^2 Q_3^2)](1 + \delta Q_3^2) \ . \tag{70}$$

Within the errors of NA22, the resulting parameters r_2 and λ_2 do not contradict those of the two-particle correlations and, therefore, are consistent with Eq. (67) and, therefore, with incoherent production of pions. DELPHI and OPAL unfortunately did not make use of this possibility, but L3 did [131].

Fig. 18 gives $\cos\phi$ (Eq. (67)) as a function of Q_3 for the case that the cumulants K_2 and K_3 are parametrized in terms of a first-order Edgeworth expansion of a Gaussian. The L3 result is consistent with $\cos\phi = 1$ for all Q_3 and, therefore, with full incoherence.

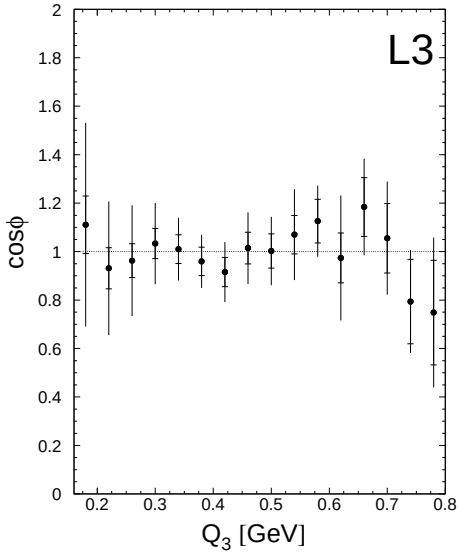


Fig. 18. $\cos\phi$ as a function of Q_3 assuming R_2 is described by the first-order Edgeworth expansion of the Gaussian [131].

Three-pion correlations have also been studied in heavy-ion collisions [132, 133] and $\langle\cos\phi\rangle = 0.20 \pm 0.02 \pm 0.19$, *i.e.* no genuine three-particle correlations are found outside the (large) errors for SPb [133]. The authors interprete this result as evidence for partial coherence [133].

What is particularly remarkable, however, is that the same experiment (NA44) with the same methodology finds an average $\langle\cos\phi\rangle = 0.85 \pm 0.02 \pm 0.21$ for PbPb collisions [133] and that this is supported by a value of $\langle\cos\phi\rangle = 0.606 \pm 0.005 \pm 0.179$ earlier reported by WA98 [132].

So, if we trust NA44 (and I have no reason not to) and try to stick with conventional pion interferometry, we end with a beautiful dilemma:

(i) e^+e^- collisions are consistent with fully incoherent pion production ($\cos\phi \sim 1$)!

(ii) SPb collisions are consistent with coherent production ($\cos\phi \sim 0$)!

(iii) PbPb is somewhere in between!

It could not be more opposite to any reasonable expectation from conventional interferometry [134]. The hint for an alternative interpretation comes from a comparison of Eqs. (67) and (46). What conventional interferometry calls the cosine of a phase has in fact nothing to do with a phase. It is simply the ratio of K_3 and twice $K_2^{3/2}$. It may be a challenge for the string model to explain why this is unity for an e^+e^- string. If that can be explained, the rest looks easy and very much in line with the behavior of the strength parameter λ discussed at the end of Sect. 4.5: The ratio $\cos\phi \sim K_3/2K_2^{3/2}$ decreases with the number of independent sources N like $N^2/2N^{3/2} \propto N^{1/2}$. As λ does, it decreases with increasing atomic mass number A up to SPb collisions. The saturation or increase of λ at and above this A has been explained by percolation [109] of strings in Sect. 4.5. Exactly the same explanation can be used to understand an increase of the ratio (not the phase!) $\cos\phi$ between SPb and PbPb collisions.

5. Conclusions

In view of possible inter-W Bose–Einstein Correlations distorting fully hadronic WW final states in e^+e^- collisions, the state of the art has been summarized on Bose–Einstein correlations in Z fragmentation. Where not (yet) available from the Z, information has been borrowed from other types of reactions. We consider this experimental information a major challenge to existing and future models.

1. Bose–Einstein correlations definitely exist in Z fragmentation. There is no reason that they should not exist within a single W (intra-W BEC). To understand possible presence or absence of BEC between pions originating from different W's (inter-W BEC), profound knowledge of BEC in the high statistics Z fragmentation data is obligatory.

2. The correlation is far from spherically symmetric. The correlation domain (defined by the lengths of homogeneity in three space directions) is elongated along the event axis. Because of strong space-momentum correlations, this elongation is small, however, as compared to the length of the total string.

3. The correlation is far from Gaussian. Good results have been obtained with an Edgeworth expansion, but even power-law behavior is not excluded.

4. A $1/\sqrt{m}_{\mathrm{T}}$ scaling first observed in heavy-ion collisions is now also observed in Z fragmentation and may suggest a "transverse" flow even there.

5. Dilution of correlations in high-multiplicity hh and AA collisions suggests the lack of cross talk between neighboring strings at low density of strings, but percolation may set in at the highest densities.

6. The full emission function in space–time can be extracted from a combination of inclusive single-particle distributions and BE correlation functions. So far, this has only be done in hh and AA collisions, in the framework of a model for three-dimensional hydrodynamic expansion. While a Gaussian shaped fire*ball* is observed for AA collisions, a fire*tube* is observed for hh collisions. A study of e^+e^- collisions is under way.

7. Consistently with the expectation from the string model, the radius for $\pi^0\pi^0$ correlations is found to be smaller than that for $\pi^\pm\pi^\pm$ correlations.

8. Genuine three-particle correlations exist in Z fragmentation and, according to conventional interpretation, would allow to extract a "phase" unmeasurable in two-particle correlations. The resulting zero phase in e^+e^- is consistent with what would be expected for fully incoherent emission. Comparison to the results obtained for heavy-ion collisions, however, raises doubts on the conventional interpretation.

I would like to thank the organizers and in particular Andrzej Białas for their kind invitation to a most pleasant meeting and Tamas Csörgő for a large number of educative discussions.

REFERENCES

[1] R. Hanbury Brown, R.Q. Twiss, *Phil. Mag.* **45**, 663 (1954); *Nature* **177**, 27 (1956) and **178**, 1046 (1956).

[2] G.I. Kopylov, M.I. Podgoretskiĭ, *Sov. J. Nucl. Phys.* **15**, 219 (1972); **18**, 336 (1974) and G.I. Kopylov, *Phys. Lett.* **B50**, 472 (1974); E.V. Shuryak, *Phys. Lett.* **B44**, 387 (1973); G. Cocconi, *Phys. Lett.* **B49**, 459 (1974); M. Biyajima, *Phys. Lett.* **B92**, 193 (1980).

[3] G. Goldhaber, W.B. Fowler, S. Goldhaber, T.F. Hoang, *Phys. Rev. Lett.* **3**, 181 (1959); G. Goldhaber, S. Goldhaber, W. Lee, A. Pais, *Phys. Rev.* **120**, 300 (1960).

[4] A. Ballestrero *et al.*, Proc. Physics at LEP2, eds. G. Altarelli, T. Sjöstrand and F. Zwirner, CERN Yellow Report 96-01, 1996, V.1, p.141.

[5] L. Lönnblad, T. Sjöstrand, *Phys. Lett.* **B351**, 293 (1995), *Eur. Phys. J.* **C2**, 165 (1998).

[6] A. Bialas, R. Peschanski, *Nucl. Phys.* **B273**, 703 (1986); *Nucl. Phys.* **B308**, 857 (1988).

[7] E.A. De Wolf, I.M. Dremin, W. Kittel, *Phys. Rep.* **270**, 1 (1996).

[8] S. Pratt, *Phys. Lett.* **B301**, 159 (1993).

[9] A. Bialas, K. Zalewski, *Eur. Phys. J.* **C6**, 349 (1999) and *Phys. Rev.* **D59**, 097502 (1999).

[10] T. Csörgő, J. Zimányi, *Phys. Rev. Lett.* **80**, 916 (1998); J. Zimányi, T. Csörgő, *Heavy Ion Phys.* **9**, 241 (1999).

[11] T.N. Thiele, *Ann. Math. Stat.* **2**, 165 (1931).

[12] R. Kubo, *J. Phys. Soc. Japan* **17**, 1100 (1962).

[13] B. Kahn, G.E. Uhlenbeck, *Physica* **5**, 399 (1938).

[14] K. Huang, *Statistical Mechanics*, John Wiley and Sons, 1963.

[15] A.H. Mueller, *Phys. Rev.* **D4**, 150 (1971).

[16] M.G. Kendall, A. Stuart, *The Advanced Theory of Statistics*, Vol. 1, C. Griffin and Co., London 1969.

[17] K. Zalewski, *Acta Phys. Pol.* **B32**, 3983 (2001).

[18] H. Gyulassy, S. Kauffmann, L.W. Wilson, *Phys. Rev.* **C20**, 2267 (1979).

[19] S. Pratt, T. Csörgő, J. Zimanyi, *Phys. Rev.* **C42**, 2646 (1990); S. Chapman, U. Heinz, *Phys. Lett.* **B340**, 250 (1994).

[20] A.N. Makhlin, Yu.M. Sinyukov, *Z. Phys.* **C39**, 69 (1988).

[21] S. Chapman, J.R. Nix, U. Heinz, *Phys. Rev.* **C52**, 2694 (1995).

[22] M.G. Bowler, *Z. Phys.* **C29**, 617 (1985), *Phys. Lett.* **B180**, 289 (1986); *Phys. Lett.* **185**, 205 (1987); X. Artru, M. Bowler, *Z. Phys.* **C37**, 293 (1988) 293.

[23] B. Andersson, W. Hofmann, *Phys. Lett.* **B169**, 364 (1986).

[24] B. Andersson, *Acta Phys. Pol.* **B32**, 3993 (2001).

[25] H. Aihara *et al.* (TPC), *Phys. Rev.* **D31**, 996 (1985).

[26] P. Avery *et al.* (CLEO), *Phys. Rev.* **D32**, 2294 (1986).

[27] M. Althoff *et al.* (TASSO), *Z. Phys.* **C29**, 347 (1985); *Z. Phys.* **C30**, 355 (1986).

[28] B. Andersson, M. Ringnér, *Phys. Lett.* **B421**, 283 (1998) and *Nucl. Phys.* **B513**, 627 (1998); Š. Todorova-Nová, J. Rameš, Simulation of Bose–Einstein effect using space–time aspects of Lund string fragmentation model, Strasbourg preprint IReS97-29.

[29] P.D. Acton *et al.* (OPAL), *Phys. Lett.* **B267**, 143 (1991).

[30] P. Abreu *et al.* (DELPHI), *Phys. Lett.* **B286**, 201 (1992); *Z. Phys.* **C63**, 17 (1994).

[31] D. Decamp *et al.* (ALEPH), *Z. Phys.* **C54**, 75 (1992).

[32] M. Acciari *et al.* (L3), *Phys. Lett.* **B493**, 233 (2000).

[33] Š. Todorova-Nová, *Acta Phys. Pol.* **B32**, 3873 (2001).

[34] F. Yano, S. Koonin, *Phys. Lett.* **B78**, 556 (1978); M. Podgoretskiĭ, *Sov. J. Nucl. Phys.* **37**, 272 (1983).

[35] G. Bertsch, M. Gong, M. Tohyama, *Phys. Rev.* **C37**, 1896 (1988).

[36] T. Csörgő, S. Pratt, Proc. Workshop on Relativistic Heavy-Ion Physics, eds. Csörgő *et al.*, KFKI-1991-28/A, Budapest 1991, p.75.

[37] U. Heinz *et al.*, *Phys. Lett.* **B382**, 181 (1996).

[38] T. Csörgő, S. Nickerson, D. Kiang, `hep-ph 9611275`, Proc. 7th Int. Workshop on Correlations and Fluctuations, eds. Hwa *et al.*, World Scientific, Singapore 1997, p.50; T. Csörgő, B. Lörstad, *Proc. XXVth Int. Symp. on Multiparticle Dynamics*, eds. D. Bruncko *et al.*, World Scientific, Singapore 1997, p. 661.

[39] S. Jadach, K. Zalewski, *Acta Phys. Pol.* **B28**, 1363 (1997).

[40] K. Fiałkowski, R. Wit, *Z. Phys.* **C74**, 145 (1997).

[41] V. Kartvelishvili, R. Kvatadze, R. Møller, *Phys. Lett.* **B408**, 331 (1997).

[42] H. Becker *et al.* (NA44 Coll.), *Z. Phys.* **C64**, 209 (1994) and *Phys. Rev. Lett.* **74**, 3340 (1995).

[43] D. Ferenc *et al.* (NA35 Coll.), *Nucl. Phys.* **A544**, 531c (1992); Th. Alber *et al.* (NA35 Coll.), *Z. Phys.* **C66**, 77 (1995).

[44] N.M. Agababyan *et al.* (NA22 Coll.), *Z. Phys.* **C59**, 195 (1993); *Z. Phys.* **C66**, 409 (1995); *Z. Phys.* **C71**, 405 (1996); *Phys. Lett.* **B422**, 359 (1998).

[45] M. Acciarri *et al.* (L3), *Phys. Lett.* **B458**, 517 (1999).

[46] P. Abreu *et al.* (DELPHI), *Phys. Lett.* **B471**, 460 (2000).

[47] G. Abbiendi *et al.* (OPAL), *Z. Phys.* **C16**, 423 (2000).

[48] S. Chapman, P. Scotto, U. Heinz, *Phys. Rev. Lett.* **74**, 4400 (1995); *Heavy Ion Physics* **1**, 1 (1995); S. Chapman, J.R. Nix, U. Heinz, *Phys. Rev.* **C52**, 2694 (1995).

[49] T. Sjöstrand, *Comput. Phys. Commun.* **82**, 74 (1994).

[50] K. Fiałkowski, R. Wit, *Acta Phys. Pol.* **B32**, 1233 (2001).

[51] A. Białas, A. Krzywicki, *Phys. Lett.* **B354**, 134 (1995); K. Fiałkowski, R. Wit, J. Wosiek, *Phys. Rev.* **D58**, 094013 (1998).

[52] K. Kolehmainen, M. Gyulassy, *Phys. Lett.* **B180**, 203 (1986).

[53] M.G. Bowler, *Particle World* **2**, 1 (1991).

[54] J.D. Bjorken, *Phys. Rev.* **D27**, 140 (1983).

[55] X. Artru, G. Menessier, *Nucl. Phys.* **B70**, 93 (1974).

[56] A. Białas, *Nucl. Phys.* **A545**, 285c (1992) and *Acta Phys. Pol.* **B23**, 561 (1992).

[57] N.M. Agababyan *et al.* (NA22), *Z. Phys.* **C59**, 405 (1993).

[58] N. Neumeister *et al.* (UA1), *Z. Phys.* **C60**, 633 (1993); H.C. Eggers, B. Buschbeck, P. Lipa, *Proc. XXVth Int. Symp. on Multiparticle Dynamics*, eds. D. Bruncko *et al.*, World Scientific, Singapore 1996, p.650.

[59] M.R. Adams *et al.* (E665), *Phys. Lett.* **B308**, 418 (1993).

[60] C. Adloff *et al.* (H1), *Z. Phys.* **C75**, 437 (1997).

[61] N.M. Agababyan *et al.* (NA22), *Z. Phys.* **C68**, 229 (1995).

[62] M. Biyajima *et al.*, *Progr. Theor. Phys.* **84**, 931 (1990); *Progr. Theor. Phys.* **88**, 157A (1992).

[63] H.C. Eggers, P. Lipa, B. Buschbeck, *Phys. Rev. Lett.* **79**, 197 (1997).

[64] I.V. Andreev, M. Plümer, R.M. Weiner, *Int. J. Mod. Phys.* **A8**, 4577 (1993).

[65] S. Hegyi, T. Csörgő, Proc. Budapest Workshop on Relativistic Heavy Ion Collisions, eds. T. Csörgő *et al.* (KFKI-1993-11/A, Budapest, 1991) p. 47; T. Csörgő, *Proc. Cracow Workshop on Multiparticle Production*, eds. A. Białas *et al.*, World Scientific, Singapore 1994 p.175; T. Csörgő, S. Hegyi, *Phys. Lett.* **B489**, 15 (2000).

[66] T. Åkesson *et al.* (AFS), *Z. Phys.* **C36**, 517 (1987).

[67] K. Kulka, B. Lörstad, *Z. Phys.* **C45**, 581 (1990).

[68] T. Abbott *et al.* (E802), *Phys. Rev. Lett.* **69**, 1030 (1992).

[69] B. Lörstad (NA44), Proc. Budapest Workshop on Relativistic Heavy Ion Collisons, eds. T. Csörgő *et al.*, KFKI-1993-11/A, Budapest 1993 p.36.

[70] T. Csörgő, B. Lörstad, *Phys. Rev.* **C54**, 1390 (1996).

[71] T. Åkesson *et al.* (AFS), *Phys. Lett.* **B129**, 269 (1983); **B155**, 128 (1985); **B187**, 420 (1987).

[72] M. Aguilar-Benitez *et al.* (NA27), *Z. Phys.* **C54**, 21 (1992).

[73] H. Beker *et al.* (NA44), *Z. Phys.* **C64**, 209 (1994); H. Beker *et al.* (NA44), *Phys. Rev. Lett.* **74**, 3340 (1995); G. Bearden *et al.* (NA44), *Phys. Rev.* **C58**, 1656 (1998).

[74] Y. Akiba *et al.* (E802), *Phys. Rev. Lett.* **70**, 1057 (1993).

[75] P. Abreu *et al.* (DELPHI), *Phys. Lett.* **B379**, 330 (1996).

[76] G. Abbiendi *et al.* (OPAL), CERN-EP/99-163, submitted to *Eur. Phys. J.* **C**.

[77] G. Alexander *et al.* (OPAL), *Z. Phys.* **C72**, 389 (1996).

[78] P.D. Acton *et al.* (OPAL), *Phys. Lett.* **B298**, 456 (1993); R. Akers *et al.*, *Z. Phys.* **C67**, 389 (1995).

[79] D. Buskulic *et al.* (ALEPH), *Z. Phys.* **C64**, 361 (1994).

[80] H. Lipkin, *Phys. Lett.* **B219**, 474 (1989); *Phys. Rev. Lett.* **69**, 3700 (1992); G. Alexander, H.J. Lipkin, *Phys. Lett.* **B456**, 270 (1999).

[81] A.M. Cooper *et al.*, *Nucl. Phys.* **B139**, 45 (1978).

[82] P. Abreu *et al.* (DELPHI), *Phys. Lett.* **B323**, 242 (1994).

[83] G. Alexander, H.J. Lipkin, *Phys. Lett.* **B352**, 162 (1995); R. Lednický, On correlation and spin composition techniques, MPI-PhE-10, 1999.

[84] G. Alexander *et al.* (OPAL), *Phys. Lett.* **B384**, 377 (1996).

[85] R. Barate *et al.* (ALEPH), *Phys. Lett.* **B475**, 395 (2000).

[86] DELPHI Collab., XXIX Int. Conf. on High Energy Physics, Vancouver 1998 (paper 154).

[87] T. Csörgő, B. Lörstad, J. Zimányi, *Z. Phys.* **C71**, 491 (1996).

[88] G. Alexander, I. Cohen, E. Levin, *Phys. Lett.* **B452**, 159 (1999); G. Alexander, *Phys. Lett.* **B506**, 45 (2001).

[89] M. Smith, *Phys. Lett.* **B477**, 141 (2000).

[90] B. Lörstad, O.G. Smirnova, *Proc. 7th Int. Workshop on Multiparticle Production*, Nijmegen, eds. R.C. Hwa *et al.*, World Scientific, Singapore 1997, p.42.

[91] A. Białas, K. Zalewski, *Acta Phys. Pol.* **B30**, 359 (1999); T. Csörgő, J. Zimányi, *Nucl. Phys.* **A517**, 588 (1990).

[92] J.J. Lu *et al.*, *Phys. Rev. Lett.* **46**, 989 (1981).

[93] A. Bamberger *et al.* (NA35), *Z. Phys.* **C38**, 79 (1988).

[94] S. Barshay, *Phys. Lett.* **B130**, 220 (1983).

[95] C. de Marzo *et al.* (NA5), *Phys. Rev.* **D29**, 363 (1984).

[96] M. Goossens *et al.*, *Nuovo Cim.* **48A**, 469 (1978).

[97] M. Adamus *et al.* (NA22), *Z. Phys.* **C37**, 347 (1988).

[98] A. Breakstone *et al.* (ABCDHW), *Phys. Lett.* **B162**, 400 (1985) and *Z. Phys.* **C33**, 333 (1987).

[99] C. Albajar *et al.* (UA1), *Phys. Lett.* **B226**, 410 (1989).

[100] T. Alexopoulos *et al.* (E735), *Phys. Rev.* **D48**, 1931 (1993).

[101] S. Y. Fung *et al.*, *Phys. Rev. Lett.* **41**, 1592 (1978).

[102] P. Lipa, H.C. Eggers, B. Buschbeck, *Phys. Rev.* **D53**, R4711 (1996).

[103] B. Buschbeck, H.C. Eggers, P. Lipa, *Phys. Lett.* **B481**, 187 (2000); B. Buschbeck, H.C. Eggers, *Nucl. Phys.* **B** (Proc. Suppl.) **92**, 235 (2001).

[104] P. Lipa, B. Buschbeck, *Phys. Lett.* **B223**, 465 (1989).

[105] A. Capella, U. Sukhatme, C.-I. Tan, J. Tran Thanh Van, *Phys. Rep.* **236**, 225 (1994).

[106] G. Alexander, E.K.G. Sarkisyan, *Phys. Lett.* **B487**, 215 (2000).

[107] T.C. Awer *et al.* (WA80), *Z. Phys.* **C96**, 67 (1995).

[108] M. Biyajima, N. Suzuki, G. Wilk, Z. Włodarczyk, *Phys. Lett.* **B386**, 297 (1996).

[109] F. del Moral, C. Pajares, *Nucl. Phys.* **B** (Proc. Suppl.) **92**, 95 (2001).

[110] S.V. Akkelin, Yu.M. Sinyukov, *Z. Phys.* **C72**, 501 (1996).

[111] T. Csörgő, *Phys. Lett.* **B347**, 354 (1995).

[112] T. Csörgő, B. Lörstad, J. Zimányi, *Phys. Lett.* **B338**, 134 (1994).

[113] B.R. Schlei, U. Ornik, M. Plümer, R.M. Weiner, *Phys. Lett.* **B293**, 275 (1992).

[114] H. Beker *et al.* (NA44), *Z. Phys.* **C64**, 209 (1994).

[115] N.M. Agababyan *et al.* (NA22), *Z. Phys.* **C71**, 405 (1996).

[116] N.M. Agababyan *et al.* (NA22), *Phys. Lett.* **B422**, 359 (1998).

[117] A. Ster, T. Csörgő, B. Lörstad, *Nucl. Phys.* **A661**, 419 (1999).

[118] T. Csörgő in *Proc. Particle Production Spanning MeV and TeV Energies*, eds. W. Kittel, P.J. Mulders, O. Scholten, NATA Science Series, 2000, p.203; *Heavy Ion Phys.* **15**, 1 (2002).

[119] T. Csörgő, *Simple Analytic Solution of Fireball Hydrodynamics*, nucl-th/9809011.

[120] D. Alde *et al.* (GAMS), *Phys. Lett.* **B397**, 350 (1997).

[121] K. Eskreys, *Acta Phys. Pol.* **36**, 237 (1969).

[122] V.G. Grishin *et al.*, *Sov. J. Nucl. Phys.* **47**, 278 (1988).

[123] P. Achard *et al.* (L3), *Bose–Einstein Correlations of Neutral and Charged Pions in Hadronic Z Decays*, to be published in *Phys. Lett.* **B**.

[124] B. Lörstad, *Int. J. Mod. Phys.* **A4**, 2861 (1989).

[125] R.M. Weiner, *Phys. Lett.* **B232**, 278 (1989); **242**, 547 (1990); V.L. Lyuboshitz, *Sov. J. Nucl. Phys.* **53**, 514 (1991).

[126] H. Heiselberg, A.P. Vischer, NBI-97-32, July 1997, U. Heinz, Q. Zhang, *Phys. Rev.* **C56**, 426 (1997).

[127] N.M. Agababyan *et al.* (NA22), *Phys. Lett.* **B332**, 458 (1994).

[128] P. Abreu *et al.* (DELPHI), *Phys. Lett.* **B355**, 415 (1995).

[129] K. Ackerstaff *et al.* (OPAL), *Eur. Phys. J.* **C5**, 239 (1998).

[130] L. Lönnblad, T. Sjöstrand, *Phys. Lett.* **B351**, 293 (1995).

[131] L3 Collab., J.A. van Dalen, W. Kittel, W. Metzger, Three-Particle Bose–Einstein Correlations in Hadronic Z Decay, submitted to 31st Int. Symp. on Multiparticle Dynamics, Datong (China), Sept. 2001.

[132] M.M. Aggarwal *et al.* (WA98), *Phys. Rev. Lett.* **85**, 2895 (2000).

[133] H. Bøggild *et al.* (NA44), *Phys. Lett.* **B544**, 77 (1999); I.G. Bearden *et al.* (NA44), *Phys. Lett.* **B517** (2001) 25.

[134] I would like to thank Š. Todorova-Nová for encouraging discussion on this point.